

Envelope Expansion with Core Collapse.

I. Spherical Isothermal Similarity Solutions

Yu-Qing Lou^{1,2,3} and Yue Shen¹

¹*Physics Department, The Tsinghua Center for Astrophysics, Tsinghua University, Beijing 100084, China*

²*Department of Astronomy and Astrophysics, The University of Chicago, 5640 S. Ellis Ave., Chicago, IL 60637, USA*

³*National Astronomical Observatories, Chinese Academy of Sciences, A20, Datun Road, Beijing 100012, China.*

Accepted 200?...; Received 2003 ...; in original form 2003 September 19

ABSTRACT

We investigate self-similar dynamical processes in an isothermal self-gravitational fluid with spherical symmetry. In reference to earlier complementary solution results of Larson, Penston, Shu, Hunter and Whitworth & Summers, we further explore the ‘semi-complete solution space’ from an initial instant $t \rightarrow 0^+$ to a final stage $t \rightarrow +\infty$. These similarity solutions can describe and accommodate physical processes of radial inflow, core collapse, oscillations and envelope expansion (namely, outflow or wind) or contraction as well as shocks. In particular, we present new classes of self-similar solutions, referred to as ‘envelope expansion with core collapse’ (EECC) solutions, that are featured by an interior core collapse and an exterior envelope expansion concurrently. The interior collapse towards the central core approaches a free-fall state as the radius $r \rightarrow 0$, while the exterior envelope expansion gradually approaches a constant radial flow speed as $r \rightarrow +\infty$. There exists at least one spherical stagnation surface of zero flow speed that separates the core collapse and the envelope outflow and that travels outward at constant speed, either subsonically or supersonically, in a self-similar manner. Without crossing the sonic critical line where the travel speed of nonlinear disturbances relative to the radial flow is equal to the sound speed, there exist a continuous band of infinitely many EECC solutions with only one supersonic stagnation point as well as a continuous band of infinitely many similarity solutions for ‘envelope contraction with core collapse’ (ECCC) without stagnation point. Crossing the sonic critical line twice analytically, there exist infinitely many discrete EECC solutions with one or more subsonic stagnation points. Such discrete EECC similarity solutions generally allow radial oscillations in the subsonic region between the central core collapse and the outer envelope expansion. In addition, we obtained complementary discrete ECCC similarity solutions that cross the sonic critical line twice with subsonic oscillations. In all these discrete solutions, subsonic spherical stagnation surfaces resulting from similarity oscillations travel outward at constant yet different speeds in a self-similar manner. With specified initial boundary or shock conditions, it is possible to construct an infinite number of such EECC similarity solutions, which are conceptually applicable to various astrophysical problems involving gravitational collapses and outflows. We mention potential applications of EECC similarity solutions to the formation process of proto-planetary nebulae connecting the AGB phase and the planetary nebula phase, to HII clouds surrounding star formation regions, and to a certain evolution phase of galaxy clusters.

Key words: hydrodynamics — planetary nebulae — stars: AGB and post-AGB — stars: formation — stars: winds, outflows — waves

1 INTRODUCTION

Hydrodynamical processes of a self-gravitational spherical gas have been investigated from different perspectives and in various contexts of astrophysical or cosmological prob-

lems on entirely different temporal and spatial scales. As an important example, solutions to the model problem of spherical gravitational collapse provide physical insights for understanding processes of star formation and outflows (Ebert

1955; Bonner 1956; Hayashi 1966; Hunter 1967; Spitzer 1968; Larson 1973; Mestel 1974). Another important field is the formation and evolution of galaxy clusters that contain massive dark matter haloes and hot gases with temperatures of $\sim 10^7 - 10^8$ K (e.g. Fabian 1994; Sarazin 1988; Gunn & Gott 1972; Bertschinger 1985; Fillmore & Goldreich 1984; Navarro, Frenk & White 1996). Detailed numerical computations to solve the fully coupled nonlinear partial differential hydrodynamic equations show that solutions, sufficiently away from initial and boundary conditions, appear to evolve into self-similar behaviours (e.g. Sedov 1959; Landau & Lifshitz 1959). Over past several decades, researchers have studied self-similar solutions under spherical symmetry and isothermal conditions. Simultaneously and independently, Penston (1969a, b) and Larson (1969a, b) found one discrete self-similar infall solution without involving a central core mass, the so-called LP-solution referred to in the literature, on the basis of their numerical calculations of spherically symmetric gravitational collapse for star formation. In addition to this LP-solution, Shu (1977) derived other types of self-similar solutions, including the so-called ‘expansion-wave collapse solution’ (with a discontinuous derivative at the sonic critical point), which leads to the physical scenario of ‘inside-out collapse’ in the context of molecular cloud and/or star formation (e.g. Shu, Adams & Lizano 1987). Shu (1977) showed clearly the existence of the sonic critical line across which two types of eigensolutions may be possibly specified.

Following Shu’s analysis, Hunter (1977) found a class of discrete ‘complete solutions’ by extending the time domain way back to the pre-catastrophic period starting from $t \rightarrow -\infty$ and by applying a zero-speed boundary condition there (see Fig. 6). One may regard the LP-solution as a special member of Hunter’s class and Shu’s expansion-wave collapse solution turns out to be a limiting case of Hunter’s solution class [see solution parameters (11) and figs. 1 and 2 of Hunter (1977)]. In terms of the ‘semi-complete solution’ structure (see Fig. 6), the ‘complete’ LP-solution and each of ‘complete’ solutions *a*, *b*, *c*, *d* and so forth of Hunter’s (1977) can be split into two branches (i.e. one inflow and one outflow) at $x \equiv r/(at) \rightarrow +\infty$. In the ‘semi-complete’ perspective, Hunter’s solutions *a*, *b*, *c*, *d* and so forth involve radial oscillations with increasing number of nodes or stagnation points in the subsonic region with either envelope expansion or envelope contraction but without initial onset of central core collapse (see Fig. 6).

Within the same overall framework of Shu (1977) and Hunter (1977), Whitworth & Summers (1985, hereafter WS) introduced more elaborate mathematical techniques to construct similarity solutions across the sonic critical line with weak discontinuities (Lazarus 1981; Hunter 1986; Ori & Piran 1988; Boily & Lynden-Bell 1995). Whitworth & Summers noted the existence of two types of sonic points (namely, saddle and nodal points defined later) in the problem (see Jordan & Smith 1977 for details) and carefully examined stability properties of numerical integration directions. They realized the distinctly different properties of

Shu’s two types of eigensolutions at the sonic critical line and referred to the two types as ‘primary’ and ‘secondary’ directions* in the case of nodal points (Jordan & Smith 1977). By allowing one solution to pass the nodal sonic point along the secondary direction and an infinite number of solutions to pass it tangentially along the primary direction as well as locally linear combinations of the two eigensolutions, WS constructed two-parameter continuum bands of solutions in addition to the previous discrete solutions. Regarding the analysis of WS, Hunter (1986) promptly pointed out that the solutions of WS involve weak discontinuities across the sonic critical line in that physical variables and all their first derivatives in space and time are continuous[†] and derivatives of some higher orders may also be continuous. Moreover, Hunter (1986) suggested that the solutions of WS may be unstable against small perturbations as numerical computations did not show tendency towards any of such solutions except for the LP-solution and therefore might not be acceptable physically. Ori & Piran (1988) proceeded to verify Hunter’s conjecture and derived a necessary stability criterion for ‘complete solutions’.

Lynden-Bell & Lemos (1988) and Lemos & Lynden-Bell (1989a, 1989b) studied self-similar solutions for a cold fluid, not only in the Newtonian regime but also in the regime of general relativity. Foster & Chevalier (1993) studied the gravitational collapse of an isothermal sphere by hydrodynamic simulations. They recovered the LP-solution in the central region where a core forms and the self-similar solutions of Shu (1977) when the ratio of initial outer cloud radius to core radius is $\gtrsim 20$. Boily & Lynden-Bell (1995) studied the self-similar solutions for radial collapse and accretion of radiative gas in the polytropic approximation. Hanawa & Nakayama (1997) also investigated the stability problem of the complete self-similar solutions in a normal mode analysis and concluded that only the LP-solution is stable. The most recent work of Harada, Maeda & Semelin (2003) studied spherical collapse of an isothermal gas fluid through numerical simulations and showed a critical behaviour for the Newtonian collapse that turns out to follow the self-similar form of the first member (i.e. solution *a*) of Hunter’s solutions (Hunter 1977).

Lai & Goldreich (2000) studied the growth of nonspherical perturbations in the collapse of a self-gravitating spherical gas cloud. They found through numerical computations that nonspherical perturbations damp in the subsonic region but grow in the supersonic region with asymptotic scaling relations for their growths. Lai & Goldreich mentioned potential applications to core-collapse of supernova explosions (Goldreich & Weber 1980; Yahil 1983), where the asym-

* For the two eigensolutions crossing the nodal sonic critical point and in terms of absolute values, the one of larger flow speed gradient is along the primary direction and the one of smaller flow speed gradient is along the secondary direction.

† This does not include those cases when a solution on one side is along the primary direction and that on the other side is along the secondary direction.

metric density perturbation may lead to asymmetric shock propagation and breakout, giving rise to asymmetry in the explosion and a kick to the new-borne neutron star. Subsequently, Lai (2000) presented a global stability analysis for a self-similar gravitational collapse of a polytropic gas.

In addition to the shock-free self-similar solutions, Tsai & Hsu (1995) found a similarity shock solution in reference to Shu's expansion-wave collapse solution through both numerical and analytical analyses for the formation of low-mass stars. Their results were recently expanded by Shu, Lizano, Galli, Cantó & Laughlin (2002) in the context of self-similar 'champagne flows' driven by a shock in HII regions. One shock solution found by Tsai & Hsu (1995) turns out to be the limiting case of many self-similar shocked LP-solutions found by Shu et al. (2002).

The perspectives of complete (Hunter 1977, 1986) and semi-complete (Shu 1977; WS) similarity solutions are both valid with proper physical interpretations and with the corresponding identification of an initial moment. In view of the invariance under the time-reversal transformation of self-gravitational fluid equations (1)–(3) below, that is, $t \rightarrow -t$, $\rho \rightarrow \rho$, $u \rightarrow -u$, the complete and semi-complete similarity solutions are closely related to each other. For example, the complete LP-solution (fig. 1 of Hunter 1977) describes a self-similar collapse process starting from the pre-catastrophic instant $t \rightarrow -\infty$ with a zero flow speed and a density distribution, passing through the sonic critical point once, gaining a finite radial infall speed at $t = 0$, and approaching eventually a free-fall state involving a central core collapse as $t \rightarrow +\infty$. However, the complete LP-solution (Hunter 1977) can be broken into two branches of similarity solution in the semi-complete space. One branch is only partially shown in the lower-left corner of Shu's fig. 2 and is described by equations (A7) and (A8) in Shu's appendix (see also Fig. 5). This branch corresponds to a self-similar outflow without core mass but with a finite central density decreasing with time t in a scaling of t^{-2} . The other branch corresponds to a constant radial inflow speed at $x \rightarrow +\infty$ and a core collapse at $x \rightarrow 0^+$ without crossing the sonic critical line. To some extent, Shu's criticism on the utility of the semi-complete LP-solution may be compromised by joining the other branch of the semi-complete LP-solution of infall-core-collapse solution (Hunter 1977) or by inserting a shock to match with an outward 'breeze' for 'champagne flows' in HII regions (Tsai & Hsu 1995; Shu et al. 2002).

With the complementarity of complete and semi-complete perspectives for self-similar solutions, we re-visit this classic problem in the semi-complete solution space with the strong motivation of finding similarity solutions for concurrent processes of central core collapse and envelope expansion or contraction that may or may not involve subsonic radial oscillations and/or shocks across the sonic critical line. Specifically, we have learned Shu's expansion-wave collapse solution as the limit of a class of core collapse solutions with zero infall speed at $x \rightarrow +\infty$. We have also noted that Hunter's complete collapse solutions, including the LP-solution, can be used to describe radial

outflows with or without subsonic radial oscillations in the semi-complete perspective. It is then physically plausible to derive self-similar solutions for concurrent envelope expansion with core collapse (EECC) that may or may not involve subsonic radial oscillations and/or shocks. If one allows solutions that pass through the sonic critical line with weak discontinuities (Lazarus 1981), then the mathematical solution space can be further expanded enormously (WS). This paper gives a positive account of constructing EECC similarity solutions that are distinctly different from known similarity solutions. With proper selections and adaptations, we believe that these EECC similarity solutions, due to their generality and simplicity, provide an important basic conceptual framework for a wide range of astrophysical problems involving gravitational collapses, outflows, contractions and subsonic radial oscillations etc. We shall mention a few potential applications, including the dynamical process of forming a proto-planetary nebula that evolves from the asymptotic giant branch (AGB) phase to the planetary nebula phase with a central hot proto white dwarf. Specifics will be described in forthcoming papers.

Several authors have approached the same set of basic isothermal fluid equations with different notations, choice of variables and conventions of presenting their results. It is sometimes mind-boggling to find correspondences among their solutions and results of analysis. Without further complications, we shall more or less adopt Shu's notations and present our results in a similar manner. The basic equations and the self-similar transformation are summarized in Section 2. In contrast to Shu's focus on the first quadrant of $-v$ versus x , we pay equal attention to both first and fourth quadrants for $-v$ versus x presentation as we are interested in both outflows and collapses. In order to place our work in a proper perspective in reference to known results, we have explored the entire solution structure, including the counterparts of those solutions found by previous authors, in Section 3. Physical interpretations for the obtained solutions are described in Section 4. We summarize and discuss our results in Section 5. Some technical details and procedures can be found in the Appendix.

2 THE BASIC MODEL FORMULATION

To be self-contained, we recount basic isothermal gravitational hydrodynamic equations with spherical symmetry below in the spherical polar coordinate (r, θ, φ) . We cast these nonlinear equations in a self-similar form (Larson 1969a; Penston 1969a; Shu 1977; Hunter 1977, 1986; Whitworth & Summers 1985) to derive useful conditions and solutions. By the spherical symmetry, the flow velocity is purely radial and the mass conservation equation is

$$\frac{\partial \rho}{\partial t} + \frac{1}{r^2} \frac{\partial}{\partial r}(r^2 \rho u) = 0, \quad (1)$$

where ρ is the gas mass density, u is the bulk radial flow speed and t is the time.

Equivalently, it is informative to rewrite equation (1) in

terms of mass enclosed in a spherical shell, namely

$$\frac{\partial M}{\partial t} + u \frac{\partial M}{\partial r} = 0, \quad \frac{\partial M}{\partial r} = 4\pi r^2 \rho, \quad (2)$$

where $M(r, t)$ is the total mass enclosed inside a sphere of radius r at time t .

In the isothermal approximation with $p = a^2 \rho$, where p is the gas pressure and a is the isothermal sound speed, the radial momentum equation then reads

$$\frac{\partial u}{\partial t} + u \frac{\partial u}{\partial r} = -\frac{a^2}{\rho} \frac{\partial \rho}{\partial r} - \frac{GM}{r^2}, \quad (3)$$

where $G \equiv 6.67 \times 10^{-8}$ dyne cm² g⁻² is the gravitational constant.

In equation (3), one identifies $-\partial\Phi/\partial r \equiv -GM(r, t)/r^2$, where $\Phi(r, t)$ is the gravitational potential. In this form, the Poisson equation for the gravitational potential Φ is automatically satisfied. The equation of energy conservation can be readily derived by combining equations (1) – (3), namely

$$\begin{aligned} \frac{\partial}{\partial t} \left\{ \frac{\rho u^2}{2} + a^2 \rho \left[\ln \left(\frac{\rho}{\rho_c} \right) - 1 \right] - \frac{1}{8\pi G} \left(\frac{\partial \Phi}{\partial r} \right)^2 \right\} \\ + \frac{1}{r^2} \frac{\partial}{\partial r} \left\{ r^2 u \rho \left[\frac{u^2}{2} + a^2 \ln \left(\frac{\rho}{\rho_c} \right) \right] \right\} \\ + \frac{1}{r^2} \frac{\partial}{\partial r} (r^2 u \rho \Phi) + \frac{1}{r^2} \frac{\partial}{\partial r} \left(\frac{r^2 \Phi}{4\pi G} \frac{\partial^2 \Phi}{\partial r \partial t} \right) = 0 \end{aligned} \quad (4)$$

(Fan & Lou 1999), where ρ_c is an arbitrary constant density scale by the mass conservation (1). One can clearly separate out two terms associated with ρ_c in the energy conservation equation (4), with the meaning of energy assigned to gas particles. For the present problem, it turns out that the last two divergence terms related to Φ on the left-hand side of equation (4) exactly cancel each other using the two expressions of equation (2). By equation (4), it is straightforward to identify the energy density \mathcal{E} and energy flux density \mathcal{F} , respectively [see definition equations (23) and (24) later].

If one were to derive similarity ‘shock conditions’ across a spatial discontinuity, the joint requirements of mass conservation (1), momentum conservation (3) and energy conservation (4) together would strictly imply continuous solutions only. That is, no simultaneous jumps in density, radial flow velocity and temperature are allowed across a spatial point in a similarity form. However in astrophysical situations (such as HII regions in molecular clouds) where radiative cooling is sufficiently fast at the shock location and the movement of shock front is sufficiently slow, one may construct ‘isothermal shocks’ (e.g. Spitzer 1978) based on mass conservation (1) and momentum conservation (3) (e.g. Courant & Friedrichs 1948) and leave radiative losses to accommodate energy conservation in a form different from equation (4).

To derive self-similar solutions of equations (1) – (3), we introduce the dimensionless independent self-similar variable $x = r/at$. Dependent variables then take the following similarity forms accordingly, namely

$$\rho(r, t) = \frac{\alpha(x)}{4\pi G t^2}, \quad M(r, t) = \frac{a^3 t}{G} m(x),$$

$$u(r, t) = av(x), \quad \Phi(r, t) = a^2 \phi(x), \quad (5)$$

where dimensionless α , m , v and ϕ are reduced variables for density, enclosed mass, radial flow speed and gravitational potential, respectively; they are functions of x only. In our formulation, $t = 0$ specifies the initial instant. Our choice of similarity variables is the same as that of Shu (1977) and of WS, while other authors may adopt different yet equivalent forms that are of the same physical nature.

Substitution of transformation equation (5) into equation (2) yields

$$m + (v - x) \frac{dm}{dx} = 0, \quad \frac{dm}{dx} = x^2 \alpha. \quad (6)$$

It follows immediately that

$$m = x^2 \alpha(x - v), \quad (7)$$

which leads to

$$\frac{d}{dx} [x^2 \alpha(x - v)] = x^2 \alpha. \quad (8)$$

For $x > 0$, the physical requirement that $m(x) > 0$ means $x - v > 0$ by equation (7). Therefore, portions of similarity solutions of $-v(x)$ and $\alpha(x)$ to the lower-left of straight line $x - v = 0$ (parallel to the sonic critical line $x - v = 1$) are unphysical.

Substitution of transformation equation (5) into equations (1) and (3) together with relation (7) yields a pair of two coupled nonlinear ordinary differential equations (ODEs), namely

$$[(x - v)^2 - 1] \frac{dv}{dx} = \left[\alpha(x - v) - \frac{2}{x} \right] (x - v), \quad (9)$$

$$[(x - v)^2 - 1] \frac{1}{\alpha} \frac{d\alpha}{dx} = \left[\alpha - \frac{2}{x} (x - v) \right] (x - v) \quad (10)$$

[see equations (11) and (12) of Shu 1977]. It is then easy to show that equation (8) can be derived from equations (9) and (10) without involving the sonic critical point at $(x - v)^2 = 1$. The main thrust of the present work is to solve the above coupled pair of nonlinear ODEs and search for new EECC self-similar solutions.

It is also straightforward to derive the Bernoulli relation along streamlines from equations (1) – (3), or equivalently, from nonlinear ODEs (9) and (10), namely

$$f(x) - x \frac{df}{dx} + \frac{v(x)^2}{2} + \ln \alpha(x) + \phi(x) = \text{constant}, \quad (11)$$

where $f(x)$ and $\phi(x)$ are functions of x only and satisfy the following two relations

$$\frac{df}{dx} = v(x) \quad \text{and} \quad \frac{d\phi}{dx} = \frac{m(x)}{x^2} = \alpha(x - v), \quad (12)$$

respectively. Since $m(x) > 0$ for $x > 0$, the reduced gravitational potential $\phi(x)$ is a monotonically increasing function of x .

3 SELF-SIMILAR SOLUTIONS OF ISOTHERMAL GAS FLOWS

All information of self-gravitational spherical isothermal similarity flows is contained in the nonlinear ODEs summa-

rized in the preceding section. Our primary focus is to derive and analyze possible similarity solutions of nonlinear ODEs (9) and (10) and their properties. In general, these similarity solutions can describe radial outflows (winds), inflows (contractions), oscillations, collapses (infalls) with or without shocks (including weak discontinuities etc.) and with or without central singularities at $x \rightarrow 0^+$. Before proceeding, it would be important to clarify several relevant concepts. We search for continuous solutions of both reduced velocity $v(x)$ and reduced density $\alpha(x)$ as functions of the independent similarity variable x ; the reduced enclosed mass $m(x)$ and the reduced gravitational potential $\phi(x)$, as well as other pertinent physical variables can be obtained accordingly.

In this paper, we shall take the range of the independent similarity variable x to extend from $x \rightarrow +\infty$ to the origin $x \rightarrow 0^+$. Such similarity solutions are referred to as ‘semi-complete solutions’ (WS) in contrast to the ‘complete solutions’ (Hunter 1977) that range from $x \rightarrow -\infty$ to $x \rightarrow +\infty$. Since $x \equiv r/(at)$, at a given instant $t > 0$, we have the entire radial range of r , while at a given radial location r , we have the entire temporal range of $t > 0$. For example, the range of $x \rightarrow +\infty$ to $x = 0$ may correspond the initial instant of $t = 0$ when the core begins to collapse to the final epoch $t \rightarrow +\infty$. On the other hand, the ‘complete solutions’ (Hunter 1977) extend back to the pre-catastrophic era from $t \rightarrow -\infty$ to $t = 0$. One major advantage of considering ‘semi-complete solutions’ is that the boundary condition of zero flow speed at $t \rightarrow -\infty$ becomes unnecessary. It is then possible to construct more physical solutions of interest with various initial conditions at $t \rightarrow 0^+$ and boundary conditions at $r \rightarrow 0$. As the relevant nonlinear ODEs here can be satisfied under the time-reversal transformation: $x \rightarrow -x$, $v \rightarrow -v$, $\alpha \rightarrow \alpha$ and $m \rightarrow -m$, the ‘complete solutions’ and ‘semi-complete solutions’ relate to each other as will be discussed later. Moreover, the time reversal transformation can also lead to different interpretations and/or applications of self-similar solutions.

3.1 Special Analytical Solutions

A straightforward exact analytical solution of nonlinear ODEs (9) and (10) is the similarity solution

$$v = 0, \quad \alpha = \frac{2}{x^2}, \quad m = 2x, \quad \frac{d\phi}{dx} = \frac{2}{x}, \quad (13)$$

which describes a hydrostatic state of a spherical system (Ebert 1955; Bonner 1956; Chandrasekhar 1957; Shu 1977). Note that equation (10) with $v = 0$ gives a solution of $\alpha = 2/(Cx^2 + 1 - C)$ where C is an integration constant. Independently, according to equations (7) and (8) with $v = 0$, one derives $\alpha = C'/x^2$ where C' is another integration constant. The two integration constants C and C' can be chosen (i.e. $C = 1$ and $C' = 2$) such that the two $\alpha(x)$ solutions are consistent with each other. For a composite spherical flow system of two isothermal fluids under self-gravity, such type of similarity solutions does not exist, even though a hydrostatic solution in a composite system does exist (Lou et al. 2003, in preparation).

Another exact analytical similarity solution of nonlinear ODEs (9) and (10) is

$$v = \frac{2}{3}x, \quad \alpha = \frac{2}{3}, \quad m = \frac{2}{9}x^3, \quad \frac{d\phi}{dx} = \frac{2}{9}x, \quad (14)$$

(WS) that passes the sonic critical line at $x_* = 3$ and that represents an expanding outflow with v approaches infinity as $x \rightarrow +\infty$. Such type of exact solutions also exist in a composite system of two isothermal fluid spheres coupled by self-gravity (Lou et al. 2003, in preparation). It is interesting to note that this solution actually corresponds to a nonrelativistic Hubble expansion in the model of the Einstein-de Sitter universe (e.g. Shu et al. 2002). In dimensional form, a pertinent Hubble ‘constant’ here is $H = 2/(3t)$ and a critical mass density is $\rho = 3H^2/(8\pi G) = 1/(6\pi Gt^2)$.

Another explicit solution is the singular solution

$$x - v = 1, \quad \alpha(x) = 2/x. \quad (15)$$

[The conjugate set of $x - v = -1$ and $\alpha(x) = -2/x$ is not considered here due to the requirement of $\alpha(x) \geq 0$. The situation would be different in a time reversal problem; see Hunter 1977]. Apparently, such a singular solution does not satisfy equation (8) and is not a real solution to the problem. It does set a requirement for sensible solutions that pass smoothly across the sonic critical line at $x - v = 1$. We will describe below more specifically the way of passing through a sonic critical point smoothly.

3.2 Asymptotic Solution Behaviours

Except for the non-relativistic Einstein-de Sitter solution (14), a reasonable assumption is that when x goes to infinity the reduced radial velocity $v(x)$ should approach a finite value[‡]. Such similarity solutions can describe either outflows with $v(x) > 0$ or inflows with $v(x) < 0$ or quasi-static or ‘breeze’ state $v(x) \rightarrow 0$ at large radii (i.e. $x \rightarrow +\infty$).

One readily derives from nonlinear ODEs (9) and (10) asymptotic solutions at large radii

$$v = V + \frac{2-A}{x} + \frac{V}{x^2} + \frac{(A/6-1)(A-2) + 2V^2/3}{x^3} + \dots, \\ \alpha = \frac{A}{x^2} + \frac{A(2-A)}{2x^4} + \frac{(4-A)VA}{3x^5} + \dots, \quad (16)$$

where V and A are two independent constants.[§] These asymptotic solutions are more general than those of Shu (1977) which can be recovered by simply setting $V = 0$.

Similarly, we derive two types of asymptotic solutions when approaching the origin $x = 0$, either

$$v \rightarrow -(2m_0/x)^{1/2}, \quad \alpha \rightarrow [m_0/(2x^3)]^{1/2}, \quad m \rightarrow m_0, \quad (17)$$

[‡] In Shu (1977), the condition that the reduced radial velocity $v(x)$ vanishes as $x \rightarrow +\infty$ was specified for his collapse solutions (without crossing the sonic critical line) with the ‘expansion-wave collapse’ as the limiting solution.

[§] Note that asymptotic solution (3.8) of WS contains a typo, that is, their $4y_\infty$ should be replaced by $4y_\infty^2$.

or

$$v \rightarrow \frac{2}{3}x, \quad \alpha \rightarrow B, \quad m \rightarrow Bx^3/3, \quad (18)$$

where m_0 and B are two constants (WS). The first asymptotic solution (17) for $x \rightarrow 0^+$ describes a central free-fall state during a self-similar collapse, with a finite core mass that increases with time and a diverging gravitational potential that steepens with increasing time. The second asymptotic solution (18) for $x \rightarrow 0^+$ does not involve central core mass and has a finite gravitational potential that becomes shallower with increasing time. Both types of $x \rightarrow 0^+$ solutions can be matched with outflow or contraction solutions at large x with or without subsonic radial oscillations. Solution (18) also corresponds to an infall or collapse in a time reversal problem. We note that solution (18) with $x \rightarrow 0^-$ is in fact the no-flow boundary condition as $t \rightarrow -\infty$ for the ‘complete solutions’ of Hunter (1977) and subsequent papers.

Asymptotic solutions (16)–(18) are extremely valuable for estimating compatible values of $v(x)$ and $\alpha(x)$ when performing numerical integrations to obtain similarity solutions starting from either $x \rightarrow +\infty$ or $x \rightarrow 0^+$.

We now consider solution behaviours in the vicinity of the sonic critical line. Except for inserting shocks across the sonic critical line to match two different branches of isothermal similarity solutions (Tsai & Hsu 1995; Shu et al. 2002), similarity solutions are physically acceptable when condition (15) is met across the sonic critical point at $x - v = 1$. As already noted (Shu 1977; Hunter 1977, 1986; WS), the sonic critical line separates subsonic regions, where the flow is subsonic relative to the similarity profile, from supersonic regions, where the flow is supersonic. Two types of sonic points can be identified. In our notations, the sonic points with $0 < x_* < 1$ in the first quadrant are all saddle points, while those with $x_* > 1$ in the fourth quadrant are all nodal points (Jordan & Smith 1977).

In general, there exist two types of eigensolutions at one sonic critical point with their first derivatives being computed by L’Hôpital’s rule[¶], namely

$$\left. \frac{dv}{dx} \right|_{x=x_*} = 1 - \frac{1}{x_*}, \quad \left. \frac{d\alpha}{dx} \right|_{x=x_*} = -\frac{2}{x_*} \left(\frac{3}{x_*} - 1 \right) \quad (19)$$

for the type 1 eigensolution and

$$\left. \frac{dv}{dx} \right|_{x=x_*} = \frac{1}{x_*}, \quad \left. \frac{d\alpha}{dx} \right|_{x=x_*} = -\frac{2}{x_*^2} \quad (20)$$

for the type 2 eigensolution. Our classification here follows that of Shu (1977), Hunter (1977) and WS. It is then clear that the two types of derivatives of $v(x)$ are of the opposite signs for a saddle point ($0 < x_* < 1$) and are both positive for a nodal point ($x_* > 1$); they are positive and equal at

[¶] Higher-order derivatives at a sonic critical point can be readily computed. We simply list derivatives up to the third order in the Appendix. Despite typos [e.g. the z'_s in equation (3.3) of WS should be $\pm 2/x_s^2$] and different notations, the calculated derivatives here are the same as those obtained by previous authors.

$x_* = 2$ and their magnitudes reverse for $x_* > 2$. Mathematically, when the sonic point is a saddle, only eigensolutions can go across the sonic critical point; when the sonic point is a node, besides the two eigensolutions there are infinitely many solutions which can go across a nodal point tangential to the direction of the eigensolution with a larger gradient: this eigendirection is referred to as the primary direction, while the other is referred to as the secondary direction that allows only one solution to pass through. The two eigensolutions are analytic across the sonic critical point (Hunter 1977, 1986; Ori & Piran 1988). Other solutions passing through a nodal sonic point along the primary direction involve weak discontinuities (Lazarus 1981; WS; Hunter 1986; Ori & Piran 1988; Boily & Lynden-Bell 1995). Specific properties of the sonic point are detailed in Appendix A.

3.3 Numerical Solutions

We now explore and present the similarity solution structure from the perspective of ‘semi-complete solutions’ in reference to previously known solutions (Larson 1969a; Penston 1969a; Shu 1977; Hunter 1977, 1986; Whitworth & Summers 1985). As already noted earlier and will be further discussed below, there exists a correspondence between the ‘complete’ and ‘semi-complete’ solutions. In the following, we construct numerical solutions in the range from $x \rightarrow +\infty$ to $x \rightarrow 0^+$ by making use of various asymptotic similarity solutions (see subsections 3.1 and 3.2). When x approaches infinity, solutions should converge to asymptotic solution (16), while when x approaches the origin, solutions should match with either solution (17) or solution (18). Among others, those solutions without encountering the sonic critical line can be readily obtained by numerical integrations from the asymptotic solution (16) at large x . However, for those similarity solutions crossing the sonic critical line, we must take extra care to distinguish various types of similarity solutions and their analyticity across the sonic critical line.

3.3.1 Solutions without crossing the sonic critical line

It is straightforward to derive numerically those similarity solutions in the entire x range without crossing the sonic critical line. We refer to the two constant parameters V and A in asymptotic solution (16) as asymptotic radial flow speed and mass density parameters, respectively. Starting from asymptotic solution (16) for $x \rightarrow +\infty$ with the two parameters V and A specified, we use the standard fourth-order Runge-Kutta scheme to integrate nonlinear ODEs (9) and (10) from a sufficiently large x to small x . More general than the condition that $v(x)$ vanishes at $x \rightarrow +\infty$ (e.g. Shu 1977), parameter V in asymptotic solution (16) is allowed here to take either positive (outflows) or negative (inflows) values.

For comparison and for setting up the stage, we reproduce Shu’s light solid line solutions (see fig. 2 of Shu 1977) by setting $V = 0$ together with different values of $A > 2$

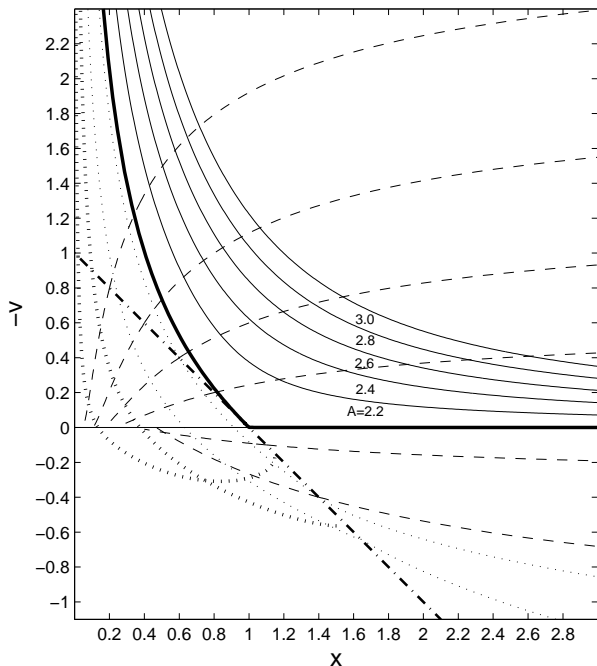


Figure 1. Representative examples of similarity solutions shown as $-v(x)$ versus x . Solutions without crossing the sonic critical line, the straight dash-dotted line for $x - v = 1$, for $V = 0$ and $A > 2$ are plotted in light solid curves, with the heavy solid curve for the ‘expansion-wave collapse’ of $A \rightarrow 2^+$ as the limiting solution. In both first and fourth quadrants, the type 1 solutions passing across the sonic critical line are plotted in dashed curves and are artificially cut off at the x axis. The special type 1 solution with $x_* = 1$ is simply static solution (13). The type 2 solutions expanded in the first quadrant with critical points are shown by dotted lines; some can go smoothly across the sonic critical line again in the fourth quadrant and extend to the right infinity, although they may not be analytic (i.e. with weak discontinuities) at the critical point in the fourth quadrant (WS; Hunter 1986). It should be noted that not all dotted lines can pass across the sonic critical line twice. We plot two such ‘unfinished’ type 2 solutions with first critical points at $x_* = 0.1$ and $x_* = 0.02$ in heavy dotted-lines as illustrating examples. Behaviours of both type 1 and type 2 solutions as $x \rightarrow +\infty$ are determined by solution (16). Some of the corresponding reduced density curves are shown in Fig. 4.

and also plot them in light solid curves in Fig. 1 as references. Such solutions have the asymptotic behaviours of solution (16) at large x and of solution (17) near the origin $x = 0$. These solutions with $A > 2$ of Shu (1977) represent self-similar collapse inflows everywhere with the fluid being at rest at infinity [$x \equiv r/(at) \rightarrow +\infty$]. Naturally, the value of the reduced core mass parameter m_0 is determined by the value of A or vice versa. The limiting solution of $V = 0$ and $A \rightarrow 2^+$ is of considerable interest in the context of star formation (e.g. Shu et al. 1987) and is shown in Fig. 1 by the heavy solid curve. This same limiting solution can also be obtained by taking the limit of $x_* \rightarrow 1^-$ where $x_* \leq 1$ is the sonic critical point in the first quadrant. This limiting solution of $-v(x)$ intersects at $x_* = 1$ where $-v = 0$, $d(-v)/dx = -1$ and joins the static singular isothermal sphere solution (13) at $x_* = 1$ with the

same reduced mass density α there. Shu (1977) referred to this special solution as the *expansion-wave collapse solution* that describes an expansion-wave front outside which the fluid is at rest and inside which the fluid collapses to form a central core. This expansion-wave front at $x \equiv r/(at) = 1$ travels outward at the isothermal sound speed a .

Shu’s ‘plus solutions’ [dashed curves with positive $d(-v)/dx$ in the first quadrant] pass through the sonic critical line at $x - v = 1$ of his (A1) type (also referred to as type 1 in the literature) and approach constant speeds at large radii ($x \rightarrow +\infty$). At large x , the reduced mass density scales as $\alpha(x) \propto x^{-2}$. At smaller $x \neq 0$ where $-v$ may become subsonic, these ‘plus solutions’ might be matched with approximate quasi-hydrostatic solutions as indicated by equations (A4) – (A6) and discussions in the Appendix of Shu (1977). Instead of time-reversed self-gravitating winds, it would be valid to regard these ‘plus solutions’ as self-similar inflows with constant speeds at large x . In addition to quasi-static matchings, it might be possible to match these self-similar inflow solutions with self-similar outflows at smaller x with or without shocks.

Shu’s ‘minus solutions’ [dotted curves with negative $d(-v)/dx$ in the first quadrant] pass through the sonic critical line at $x - v = 1$ of his (A2) type (also referred to as type 2 in the literature) and approach zero at $x < 1$. As these solutions join the static singular isothermal sphere solution (13) at $x < 1$ with smaller values of α , Shu (1977) ignored them but focused on the limiting expansion-wave collapse solution at $x_* \rightarrow 1^-$ where α can be made continuous. In the present analysis, we emphasize that these similarity solutions can be further continued in the fourth quadrant to pass through the second sonic critical point. Those solutions that pass through the sonic critical line in the fourth quadrant along the primary direction may involve weak discontinuities (Lazarus 1981; WS; Hunter 1986). There exists one solution (intersecting the x -axis once) that passes through the sonic critical line analytically in the fourth quadrant along the secondary direction. These similarity solutions are characterized by core collapse infalls for small x and envelope expansions for large x with a stagnation point at $x < 1$ that travels outward at a subsonic speed. These similarity solutions are referred to as EECC solutions (defined earlier) and will be further discussed in the context of forming planetary nebulae with central proto white dwarfs.

Only a small segment of the LP-solution is shown in the lower-left corner of fig. 2 of Shu (1977) with basic properties of LP-solution described in the paragraph containing equations (A7) and (A8). Hunter (1977) obtained a class of discrete yet infinitely many LP-type solutions in the ‘complete’ perspective. These solutions will be discussed and compared with our ‘semi-complete’ solutions later.

For numerical integrations with $V = 0$, condition $A > 2$ is necessary for self-similar solutions to exist without crossing the sonic critical line $x - v = 1$ in the first quadrant. For $V < 0$ corresponding to inflow at $x \rightarrow +\infty$, the lower limit of A such that similarity solutions exist without crossing the sonic critical line becomes less than 2. As illustrating

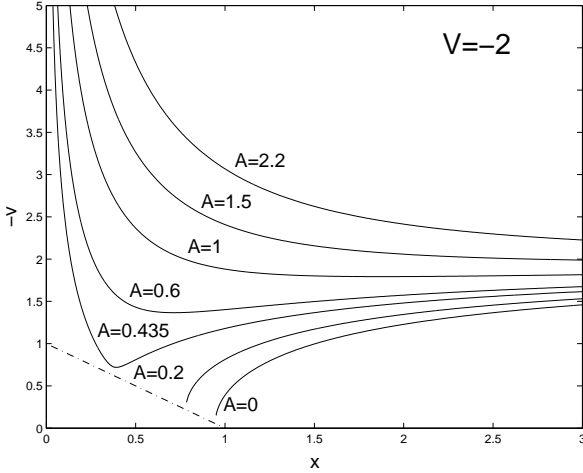


Figure 2. The class of similarity solutions integrated from a sufficiently large x for $V = -2$ with different values of A . For similarity solutions without crossing the sonic critical line, the dash-dotted line for $x - v = 1$, the lower limit of A is less than 2. For A less than this lower limit, solutions will bump into the sonic critical line; only those satisfying critical condition (15) are relevant.

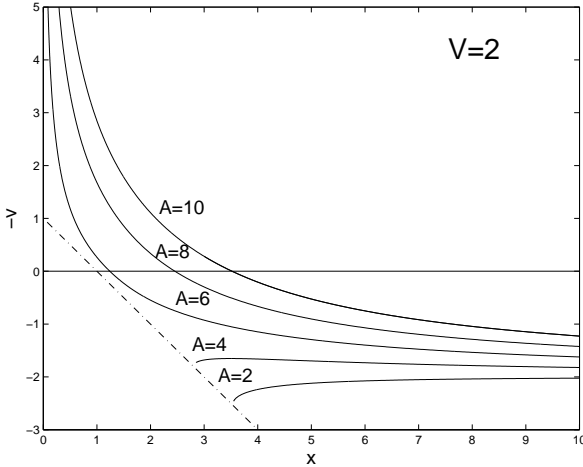


Figure 3. The class of similarity solutions integrated from a sufficiently large x for $V = 2$ with different values of A . For similarity solutions without crossing the sonic critical line, the dash-dotted line for $x - v = 1$, the lower limit of A is greater than 2. For A less than this lower limit, solutions will bump into the sonic critical line; only those satisfying critical condition (15) are relevant.

examples shown in Fig. 2, we obtained solutions through numerical integrations from large x with $V = -2$ and different values of A . When A becomes sufficiently small, similarity solutions will ‘crush’ towards the sonic critical line (e.g. the two curves labelled by $A = 0.2$ and $A = 0$). This ‘crush’ behaviour may be avoided when A becomes sufficiently large (e.g. $A > 0.435$; the more precise separation value of A lies somewhere between $A = 0.2$ and $A = 0.435$). For solutions ‘crushing’ towards the sonic critical line in Fig. 2, only those satisfying critical condition (15) in the first quadrant (saddle points) are physically valid.

Similarly, parameter V can be chosen to be positive

corresponding to a constant outflow speed as $x \rightarrow +\infty$. For different values of A , it is straightforward to integrate numerically from a sufficiently large x with asymptotic solution (16) towards the origin $x = 0$. The minimum A value for similarity solutions without crossing the sonic critical line now becomes greater than 2 in general, and varies for different values of $V > 0$. In Fig. 3, we show examples of $V = 2$ with different values of A . We emphasize that the three upper similarity solutions (i.e. $A = 6, 8, 10$) describe envelope expansions with core collapses (EECC) with the stagnation point travelling outward at a supersonic speed. The reduced core mass parameter m_0 depends upon the two parameters V and A . There exist continuous bands of such EECC similarity solutions in terms of the two parameters V and A .

We have just shown the family of similarity solutions without crossing the sonic critical line. The class of Shu’s solutions is a special case with parameter $V = 0$ in our scheme of classification. All these similarity solutions approach asymptotic condition (17) as $x \rightarrow 0^+$ with different values of m_0 that depends on both V and A . Typically, we find for the same value of V , a larger A will give a larger m_0 ; and for the same value of A , a larger V (including its sign) leads to a smaller m_0 . This can be understood as the initial density is proportional to A and the initial radial velocity is specified by V . Inflows and outflows correspond to $V < 0$ and $V > 0$, respectively. We provide physical interpretations for these similarity solutions in Section 4. Examples of different V , A and m_0 are summarized in Table 1.

In the radiative gas flow problem considered by Boily & Lynden-Bell (1995), a table is listed in their subsection 8.2 but without explicit solution figures for us to compare. Qualitatively, it appears that their results in subsection 8.2 might have some similar properties as our solutions discussed in this subsection, which do not involve the sonic critical line.

3.3.2 Solutions crossing the sonic critical line

Technically, one cannot directly obtain similarity solutions that go across the sonic critical line by numerical integration from $x \rightarrow +\infty$. For solutions satisfying critical condition (15), we expand $v(x)$ and $\alpha(x)$ in Taylor series in the vicinity of a sonic critical point denoted by x_* . For eigensolutions (e.g. Jordan & Smith 1977), we have Taylor expansions near a critical point x_* as

$$\begin{aligned}
 -v(x) &= (1 - x_*) + \left(\frac{1}{x_*} - 1\right)(x - x_*) \\
 &\quad + \frac{x_* - 1}{2x_*^2}(x - x_*)^2 + \dots, \\
 \alpha(x) &= \frac{2}{x_*} - \frac{2}{x_*} \left(\frac{3}{x_*} - 1\right)(x - x_*) \\
 &\quad + \frac{x_*^2 - 8x_* + 13}{x_*^3}(x - x_*)^2 + \dots
 \end{aligned} \tag{21}$$

for type 1 solutions, and

$$\begin{aligned}
 -v(x) &= (1 - x_*) - \frac{1}{x_*}(x - x_*) \\
 &\quad - \frac{x_*^2 - 5x_* + 5}{2x_*^2(2x_* - 3)}(x - x_*)^2 + \dots, \\
 \alpha(x) &= \frac{2}{x_*} - \frac{2}{x_*^2}(x - x_*) \\
 &\quad - \frac{x_*^2 - 6x_* + 7}{x_*^3(2x_* - 3)}(x - x_*)^2 + \dots
 \end{aligned} \tag{22}$$

for type 2 solutions (Shu 1977; Hunter 1977, 1986; Whitworth & Summers 1985). The segment of the sonic critical line in the range of $0 < x_* < 1$ in the first quadrant involves saddle points; the type 1 solutions correspond to negative first-order derivatives of $v(x)$, while the type 2 solutions correspond to positive first-order derivatives of $v(x)$ (e.g. dotted curves in the first quadrant of Fig. 1). The portion of the sonic critical line in the range of $x_* > 1$ involves nodal points and both types of eigensolutions have positive first-order derivatives of $v(x)$ across the sonic critical line.

It is straightforward to calculate higher-order derivatives at a critical point x_* (see equations A2 and A3 in Appendix A). With these in mind, we perform Taylor expansions in the vicinity of a sonic critical point to assign compatible initial values of $v(x)$ and $\alpha(x)$ and integrate along numerically stable directions. Both WS and Hunter (1986) noted that numerical integrations away from a saddle point are stable, while numerical integrations away from a nodal point are either unstable or neutrally stable (Jordan & Smith 1987)^{||}. We have been extremely careful in handling such numerical integrations across the sonic critical line, and try as much as we can to avoid those unstable backward integrations from a nodal point and use up to second-order derivatives** of Taylor expansions to estimate compatible initial values of $v(x)$ and $\alpha(x)$.

We first describe in some details the type 1 solutions. With the Taylor expansion (21) for type 1 solutions near the sonic critical line in the first quadrant, one obtains numerically a class of solutions of $v(x)$ shown in Fig. 1 denoted by dashed curves. These solutions of $v(x)$ in the first quadrant, referred to as *plus* solutions by Shu (1977), approach negative constant values of V as $x \rightarrow +\infty$. The corresponding solutions of $\alpha(x)$ scale as A/x^2 with $A < 2$ as $x \rightarrow +\infty$, consistent with the asymptotic behaviour (16) for $x \rightarrow +\infty$. Following the same procedure, we also obtain type 1 solutions which pass through the sonic critical line in the fourth quadrant. These solutions have the properties that $v(x)$ approaches a positive constant V and $\alpha(x)$ has the asymptotic behaviours of A/x^2 with $A > 2$ as $x \rightarrow +\infty$. Several

examples are shown in Table 2. We will see that a class of discrete yet infinitely many type 1 solutions satisfies requirement (18) near the origin $x = 0$. This type of solutions were first derived by Hunter (1977). Note that for $x_* = 1$, the type 1 solution reduces to the static solution (13) with $v(x) = 0$.

We next discuss the type 2 solutions across the sonic critical line. By asymptotic expansion (22) near the sonic critical point in the first quadrant, we obtain another class of self-similar solutions. Some of these solutions can go across the sonic critical line smoothly once again in the fourth quadrant (either analytically or with weak discontinuities) and approach constant values at large x . Qualitatively, such solutions bear similar features as those solid-line solutions. For comparison, we present the type 2 solutions in dotted curves in Fig. 1. Those type 2 solutions that cannot pass twice the sonic critical line are regarded as unphysical. Those type 2 similarity solutions that go across the sonic critical line twice in the first and fourth quadrants are new similarity solutions. There is yet another possibility of matching shocks across the sonic critical line in the fourth quadrant with different asymptotic solutions (e.g. Tsai & Hsu 1995; Shu et al. 2002). We shall discuss continuous self-similar solutions in Section 3.4.

3.3.3 The Larson-Penston (LP) type and the Hunter type of discrete solutions

By both numerical and analytical analyses, Larson (1969a) and Penston (1969a) independently derived a kind of monotonic similarity solution, which has the asymptotic behaviour (18) near the origin $x = 0$. The LP-type of solution can be obtained numerically by trying different values of B parameter in asymptotic solution (18) near $x = 0$ and by integrating nonlinear ODEs (9) and (10) outward from around the origin $x = 0$ towards the sonic critical line $x - v = 1$ until critical condition (15) is met such that the resulting solution matches with one of the two eigensolutions at the sonic point. Here, B is essentially an eigenvalue parameter for nonlinear ODEs (9) and (10). For the LP-solution, the eigenvalue B is ~ 1.67 . In earlier studies (Shu 1977; Hunter 1977; WS), it was found that while the LP solution is formally classified as type 2 solution (22) across the sonic critical point in the fourth quadrant, the corresponding eigensolution is in fact along the secondary direction for $x_* > 2$. That is, the LP-solution is analytic across the sonic critical line. If we relax the requirement that solutions must be analytic (as defined by Hunter 1986) across the sonic critical line, it is then possible to construct a continuum band of solutions with $0 < B < 1.67$ crossing the sonic critical line involving weak discontinuities, with the LP-solution as the limiting solution (i.e. the band 0 solutions constructed by WS with $x_* \geq 2.33$, that have no stagnation points for $0 < x < x_*$). When $x_* > 2$, the first-order derivatives of $v(x)$ for the two eigensolutions are different with $D_2 < D_1$, where D stands for the gradient of $v(x)$ at the sonic critical point and subscript numerals of D mark the types of eigen-

^{||} Numerical integrations towards a nodal point are stable, while numerical integrations away from a nodal point along the direction of eigensolutions with the smaller magnitude of the first derivative (i.e. the secondary direction) are neutrally stable (WS).
^{**} To avoid the dense singular points in higher-order derivatives (see Hunter 1986 and our Appendix A), we utilize only up to second-order derivatives and choose an appropriate step away from a nodal point to assign initial values (see Appendix A).

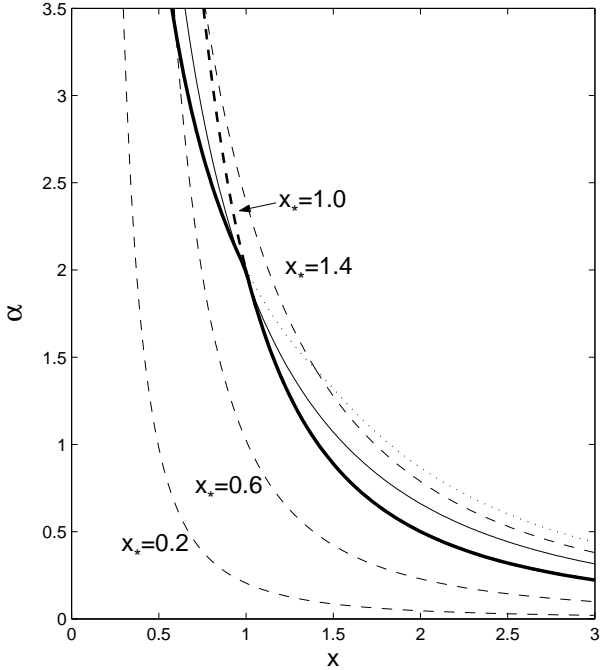


Figure 4. For the same parameters given in Fig. 1, we show here the corresponding solutions of reduced density $\alpha(x)$ by solid, dotted and dashed curves, respectively. The light solid curve is for $V = 0$ and $A = 3$ without crossing the sonic critical line. The heavy solid line corresponds to the limiting case of $V = 0$ and $A = 2^+$ (i.e. expansion-wave collapse solution). The dotted curve is for one of the type 2 solutions that passes smoothly through the sonic critical line twice (with weak discontinuities in the fourth quadrant), one at $x_* = 0.6$ and the other at $x_* = 1.395$. The dashed curves are type 1 solutions which pass through the sonic critical line in the first and fourth quadrants, respectively. The heavy dashed line is the type 1 solution with $x_* = 1$ corresponding to analytical static solution (13) of $\alpha = 2/x^2$. Specifically, the $x < 1$ portion of the heavy solid line is the limit of the dotted lines in the first quadrant as x_* approaches 1^- , while the $x > 1$ portion of the heavy solid line is approximately the static solution almost completely overlapping with the heavy dashed curve.

solutions. The LP-solution has a speed gradient equal to D_2 as it intersects the sonic critical line. Those solutions with $B \gtrsim 1.67$ have a speed gradient smaller than D_2 and thus cannot go across the sonic critical point because the required speed gradient falls within the range of $[D_2, D_1]$ (WS).

We present several such examples in Fig. 5 with both $-v(x)$ and $\alpha(x)$ shown simultaneously in the same plot [viz. $\alpha(x)$ in the upper portion and $-v(x)$ in the lower portion]. According to the solution construction scheme of WS, there should exist an infinite number of solutions fanning out from a single x_* along the primary direction across the sonic critical line that involve weak discontinuities (e.g. second-order weak shocks as noted by Boily & Lynden-Bell 1995); for each case of Fig. 5, we plot only one solution curve to the right of the sonic critical line for illustration. Besides the LP-solution with $x_* = 2.33$, the constant α solution (14) with $x_* = 3$ is also analytic at the sonic critical point. The former is along the secondary direction while the latter is along the primary direction.

In the perspective of ‘complete solutions’ ranging from $t \rightarrow -\infty$ to $t \rightarrow +\infty$ to the collapse problem, Hunter (1977) found, in addition to the LP-solution, a class of infinitely many discrete similarity solutions (see his fig. 2) that are analytic across the sonic critical line, labelled by indices ‘a’ and ‘c’, ‘b’ and ‘d’ and so forth, although he regarded the ‘a’ and ‘c’ solutions as physically invalid in the scheme of ‘complete solutions’. These solutions satisfy asymptotic condition (18) at the origin $x = 0$ and are matched with type 1 eigensolutions at the sonic critical line with $x_* < 2$ (along secondary directions). In our ‘semi-complete’ perspective, each of Hunter type discrete solutions consists of two separate branches in the first and fourth quadrants as $x \rightarrow +\infty$. The first branch, corresponding to the pre-catastrophic period (Hunter 1977) but with opposite sign of $v(x)$, is demonstrated in Fig. 6; this branch is obtained by numerically integrating from the origin $x = 0$ with B parameter specified according to expressions (11a) – (11d) of Hunter (1977) [i.e. $B = \exp(Q_0)$ where Q_0 is a parameter introduced by Hunter] to the sonic critical line and by further expanding from the right side of the sonic critical line using type 1 solution (20) along the secondary direction, until $v(x)$ approaches a constant V and $\alpha \rightarrow A/x^2$ as $x \rightarrow +\infty$. The second branch shown in Fig. 6, according to the post-catastrophic period (Hunter 1977), is obtained by specifying parameters A and $-V$ in asymptotic solution (16) and by integrating from $x \rightarrow +\infty$ back towards the origin $x = 0$. The main difference is that we focus on the first and fourth quadrants with positive x , while Hunter (1977) studied such solutions with both negative and positive time t . Hence, one complete solution such as ‘b’ in Hunter (1977), corresponds to two independent solution branches in our semi-complete solution space. For example, the first branch corresponding to the ‘b’ solution of Hunter (1977) has $|v| \rightarrow 0.295$ and $\alpha x^2 \rightarrow 2.378$ as $x \rightarrow +\infty$. By numerical integration from $x \rightarrow +\infty$ under $V = -0.295$ and $A = 2.387$, we obtain the second branch labelled by ‘b’ shown in Fig. 6 also in a heavy solid curve.

We note that Whitworth & Summers (1985) have significantly expanded Hunter’s discrete similarity solutions to separate continuous solution bands by allowing weak discontinuities at a node along the primary direction or by local linear combination of the two eigensolutions. The solution construction scheme of WS was criticized by Hunter (1986) as being non-analytic across the sonic critical line, even though such solutions are mathematically possible. Similarity solutions with weak discontinuities across the sonic critical line tend to be unstable (Hunter 1986; Ori & Piran 1988) and might bear little physical significance. In the following analysis, we mainly focus on similarity solutions that go across the sonic critical line analytically, although we mention possible similarity solutions with weak discontinuities across the sonic line for mathematical completeness.

3.4 Solutions crossing the Sonic Line Twice

We mentioned in subsection 3.3.2 that some of the type 2 solutions with $x_*(1) < 1$ in the first quadrant can extend to

$V=0$	A	2.0+	2.2	2.4	2.6	2.8	3.0
	m_0	0.976	1.45	1.885	2.311	2.743	3.186
$V=-2$	A	0.435	0.5	1.0	1.5	2.0	2.5
	m_0	0.624	0.804	2.117	3.594	5.219	6.971
$V=2$	A	6.0	7.0	8.0	9.0	10.0	11.0
	m_0	1.508	3.396	5.458	7.737	10.231	12.935

Table 1. Parameter sets of V , A and m_0 for self-similar solutions without crossing the sonic critical line (see Figs. 2 and 3).

x_*	0.2	0.4	0.6	0.8	1	1.2	1.4	1.6
V	-2.82	-1.93	-1.22	-0.59	0	0.57	1.12	1.67
A	0.177	0.468	0.864	1.374	2	2.781	3.695	4.773

Table 2. Key parameters x_* , V and A for the plus (or type 1) solutions in either first or fourth quadrant, where x_* is the location of the sonic critical point for the relevant self-similar solutions.

the fourth quadrant and satisfy again critical condition (15) when crossing the sonic critical line with $x_* > 1$. We denote the first critical point by $x_*(1)$ (less than 1) in the first quadrant and the second critical point by $x_*(2)$ (greater than 1). Such solutions, not necessarily analytic at the second critical point $x_*(2)$, can be continued across the sonic critical line towards $x \rightarrow +\infty$ in an infinite group that consists of one solution along the secondary direction and many other solutions along the primary direction. In general, this kind of solutions along the primary direction involve weak discontinuities across the sonic critical line. Meanwhile, there exist solutions that match with one of the two eigensolutions at $x_*(2)$ and that are thus analytic across the sonic critical line. It is possible to construct numerical solutions that are of the type 2 eigensolutions expanded at $x_*(1)$ in the first quadrant and that are matched with either type 1 or type 2 eigensolutions expanded at $x_*(2)$ in the fourth quadrant.

3.4.1 Solutions with weak discontinuities

We now construct those similarity solutions which can go across the sonic critical line once in the first quadrant [$x_*(1) < 1$] and again in the fourth quadrant [$x_*(2) > 1$], respectively. Apparently, such solutions must be of type 2 eigensolutions at the first critical point $x_*(1)$. There are more possibilities at $x_*(2)$ for solution matchings.

As $x_*(1)$ in the first quadrant is a saddle point, numerical integrations away from $x_*(1)$ are stable. We therefore integrate from $x_*(1)$, using Taylor expansion (22) to select initial values, towards the sonic critical line in the fourth quadrant. When critical condition (15) is met as a solution curve of $v(x)$ versus x crashes towards the sonic critical line $x - v = 1$, the solution can be extended from $x_*(2)$ further towards right with increasing x . Many of such solutions have been found to satisfy critical condition (15), although they may not be analytic at different $x_*(2)$ (WS; Hunter 1986).

In particular, an infinite group of solutions will fan out from $x_*(2)$ along the primary direction by the construction

scheme of WS. Such solutions do in fact involve weak discontinuities, and are regarded by Hunter (1986) as unphysical^{††}. Through our numerical explorations, there appear to exist a continuum of such solutions in the approximate range $0.2 < x_*(1) < 1$. When $x_*(1)$ becomes sufficiently small, the solution of $-v(x)$ will turn upward as shown in Fig. 1 [e.g. the heavy dotted-line with $x_*(1) = 0.02$]. Solution behaviours of $v(x)$ when $x_*(1)$ approaches the origin $x = 0$ will be further discussed later. Therefore, in a certain range of $x_*(1)$, integrations from $x_*(1)$ can reach the nodal region $1 < x < 2$ along the sonic critical line where backward numerical integrations from $x_*(2)$ are unstable (i.e. extremely sensitive to the accuracy of starting conditions) for type 2 solutions (along the primary direction) and are neutrally stable for type 1 solutions (along the secondary direction).

3.4.2 Self-similar solutions that are analytic across the sonic critical line

Described below is a useful numerical procedure of finding a similarity solution that is analytic across the sonic critical line (Hunter 1977). By properly specifying pertinent parameters, one integrates from a series of starting points near and alongside a portion of the sonic critical line in the first quadrant towards a chosen meeting point $x = x_F$, plots the resulting series values of functions v and α in pair at $x = x_F$ in the v -versus- α phase diagram to obtain the first locus. One then starts integrations near and alongside another portion of the sonic critical line in the fourth quadrant by specifying eigensolutions as initial values towards the same x_F and thus obtains the second locus in the $v - \alpha$ phase diagram. When the two phase loci intersect with each other, one then finds a self-similar solution that goes across the sonic critical line twice analytically. Note such an intersecting point

^{††} The physical solutions are also required to be analytic at the critical point, that is, only the two types of eigensolutions are analytic (see Hunter 1986).

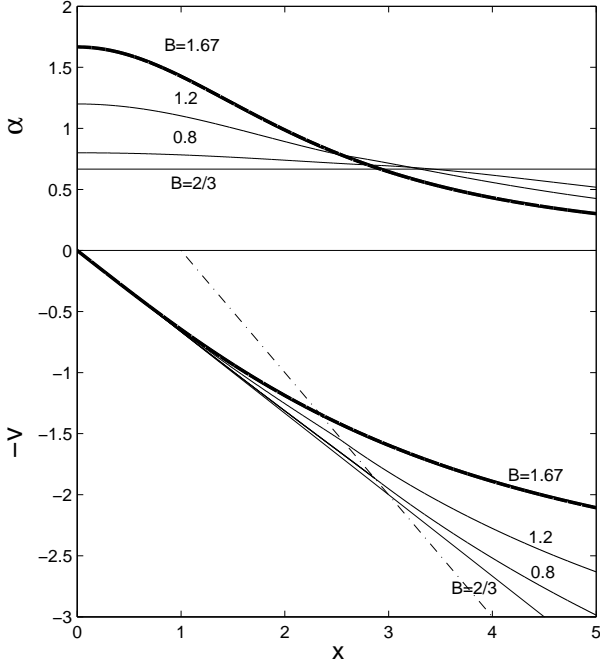


Figure 5. The LP-type solutions. The solid lines beneath the x axis are solutions of $-v(x)$ versus x , while those curves above the x axis are those of corresponding $\alpha(x)$ versus x . The sonic critical line $x - v = 1$ is denoted by the dash-dotted line below the x -axis. The pair of heavy solid curves is the LP-solution first found by Larson and Penston independently. These LP-type solutions are obtained by integrating from the origin $x = 0$ with asymptotic solution (18) and assigning different values for parameter B . Those values of B in the range $(0, 1.67]$ can all satisfy critical condition (15) (corresponding to solution band 0 with weak discontinuities of WS). The case of $B = 2/3$ corresponds to the exact analytical solution (14). As $x \rightarrow +\infty$, LP-type solutions all have the asymptotic behaviours of (16) with different parameter combinations of V and A .

in the phase diagram should be at a x -location away from the sonic critical line. The derivatives of $v(x)$ and $\alpha(x)$ are uniquely determined by the values of v and α by equations (9) and (10) for an integration point x away the sonic critical line; along the sonic critical line, there are two distinct pairs of derivatives of $v(x)$ and $\alpha(x)$ given by equations (19) and (20).

In these numerical integrations, we essentially follow the same method of Hunter (1977). The main difference is that the assigned points of Hunter are now replaced by different values of $x_*(1)$ for type 2 eigensolutions at saddle points along the sonic critical line in the first quadrant. Numerical integrations away from a saddle point $x_*(1)$ are stable and can be performed in a straightforward manner. In contrast, numerical integrations backward from a nodal point $x_*(2)$ near and alongside the sonic critical line in the fourth quadrant require extra care. In practice, we use either type 1 or type 2 eigensolutions around $x_*(2)$ up to the second-order derivatives and a carefully chosen step backward of the sonic critical line to assign initial values. We then integrate towards x_F from both $x_*(1)$ and $x_*(2)$ to search for solution matches described above. Note that the relevant values

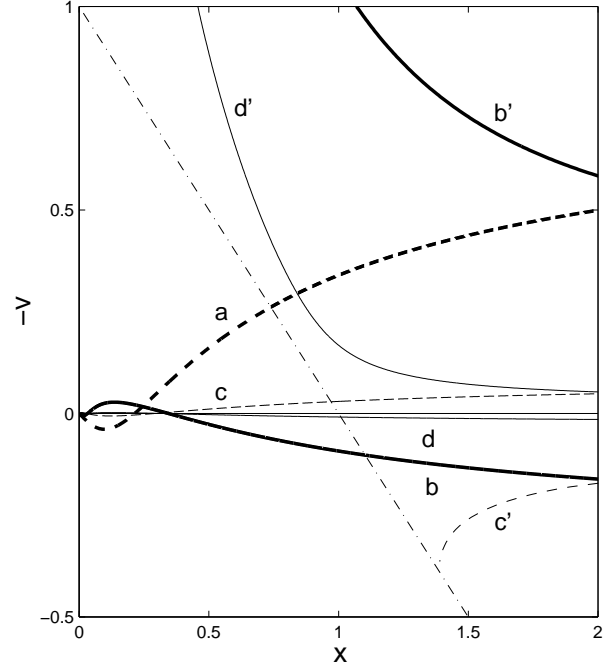


Figure 6. Each of the Hunter-type discrete ‘complete solutions’ can be broken into two branches in the first and fourth quadrants as $x \rightarrow +\infty$ in the ‘semi-complete’ scheme. Such similarity solutions are those of type 1 that satisfy condition (18) with parameter B specified by expressions (11a)-(11d) of Hunter (1977), where $B \equiv \exp(Q_0)$ and Q_0 is a parameter introduced by Hunter. Two such ‘complete solutions’, that is, the ‘b’ and ‘d’ solutions of Hunter (1977), appear as two separate branches in heavy and light solid curves, respectively. The corresponding ‘a’ and ‘c’ solutions of Hunter (1977) shown in heavy and light dashed lines have only one branch as the other branch cannot go across the sonic critical line when integrating back from $x \rightarrow +\infty$. For example, the branch marked ‘c’ cannot pass the sonic critical line smoothly. Further below the ‘c’ curve, to the lower right of the sonic critical line, would be the ‘a’ curve which is not shown here. The dash-dotted line is the sonic critical line $x - v = 1$.

of $x_*(2)$ are less than 2 as no integrations from $x_*(1)$ can reach the range of the sonic critical line with $x > 2$.

For a type 2-type 1 solution match, we choose^{‡‡} $x_F = 0.5$ and integrate from $x_*(1)$ with a type 2 eigensolution. Meanwhile, we integrate from $x_*(2)$ with a type 1 eigensolution (i.e. along the secondary direction) towards x_F . The $v - \alpha$ phase diagram at $x = x_F$ is shown in Fig. 7. The ‘spiral structure’ is strikingly similar to that in fig. 2 of Hunter (1977), the trend of which then implies an infinite number

^{‡‡} Once the meeting point x_F is chosen, only certain ranges of $x_*(1)$ and $x_*(2)$ are pertinent to a specific type of similarity solutions being searched for. Typically, values of $x_*(1)$ lie in the interval of $(0, x_F)$ and values of $x_*(2)$ cannot be too large. Otherwise, integrations away from $x_*(2)$ may not reach x_F and can become extremely sensitive to initial values along the primary direction at the sonic point. Numerical integrations from $x_*(1) \geq 0.5$ with type 2 eigensolutions in the first quadrant are found to approach $x_*(2)$ in the type 2 direction (i.e. the primary direction) and it is thus not easy to match with the type 1 eigensolutions along the sonic critical line in the fourth quadrant.

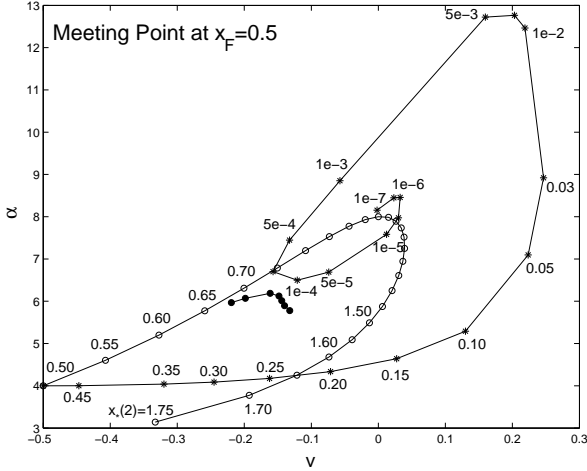


Figure 7. The phase diagram of v versus α at a chosen meeting point $x_F = 0.5$ for type 2-type 1 solution matches [that is, type 2 eigensolution at $x_*(1)$ and type 1 eigensolution at $x_*(2)$ along the secondary direction for $x_*(2) < 2$]. Each asterisk symbol * denotes an integration from $x_*(1)$ and each symbol circle \circ denotes an integration from $x_*(2)$ of a type 1 eigensolution in the fourth quadrant. The * curve and the \circ curve intersect with each other in the phase diagram. From the spiral trend of the * curve (somewhat similar to fig. 2 of Hunter 1977), we infer that there exist an infinite number of discrete type 2-type 1 self-similar solutions with the static solution (diverge at the origin) as the limiting case. The first such solution match corresponds to $x_*(1) \approx 0.23$ and $x_*(2) \approx 1.65$. We have chosen the meeting point x_F to be 0.5 here. For $x_*(1) = x_*(2) = 0.5$ with the same set of α and v in the phase diagram, there are two different sets of derivatives given by expressions (19) and (20). Despite the appearance, the phase point $(-0.5, 4)$ for (v, α) at $x_*(1) = x_*(2) = 0.5$ in this figure is therefore not a real match because the first-order derivatives are distinctly different. We add the locus of the type 2 backward integrations from $x_*(2)$ in solid circles.

of discrete type 2-type 1 self-similar solutions that can pass twice the sonic critical line analytically. The first three of such similarity solutions are displayed in the form of $-v(x)$ versus x in Fig. 10, with the enlarged part shown in Fig. 11 for small x using a logarithmic scale. It is interesting to note that the number of stagnation points, corresponding to self-similar radial oscillations, increases for such class of similarity solutions with smaller $x_*(1)$. Specifically, the first similarity solution (labelled by 1) has only one stagnation point crossing the x -axis and the relevant parameters are $x_*(1) \approx 0.23$ and $x_*(2) \approx 1.65$. The parameters of the second solution are $x_*(1) \approx 2.5858 \times 10^{-4}$ and $x_*(2) \approx 0.743$. The parameters of the third solution are $x_*(1) \approx 6 \times 10^{-6}$ and $x_*(2) \approx 1.1$.

The situation becomes somewhat involved for a type 2-type 2 solution match as $x_*(2)$ in this case is a nodal point and the type 2 eigensolutions with $x_*(2) < 2$ happen to be along the primary direction (Jordan & Smith 1977). Only within a narrow range of $x_*(2)$, can numerical solutions be integrated to reach $x_F = 0.5$. For this reason, we choose different values of x_F . First, we choose $x_F = 1$ and integrate from both $x_*(1)$ and $x_*(2)$ by type 2 eigensolution

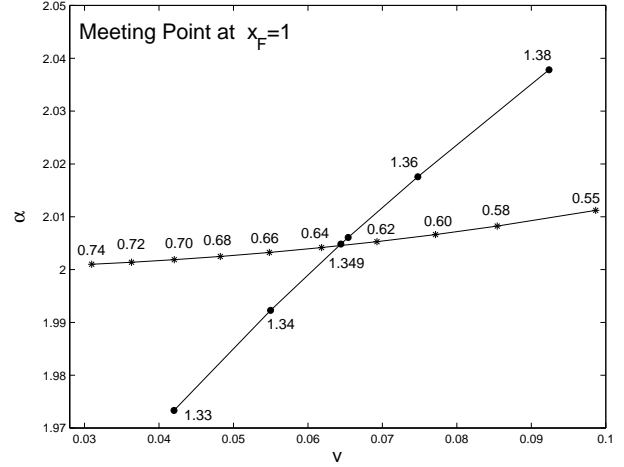


Figure 8. The phase diagram of v versus α at a chosen meeting point $x_F = 1$. Each asterisk symbol * denotes an integration from $x_*(1)$ with its value shown and each full circle denotes an integration from $x_*(2)$ with its value shown. Both integrations are of type 2 eigensolutions when crossing the sonic critical line at $x - v = 1$. There is an intersection at $x_F = 1$ in the phase diagram and thus a unique match of $v(x_F)$ and $\alpha(x_F)$ from both sides of $x_F = 1$. For this matched solution, we have $x_*(1) \approx 0.632$ and $x_*(2) \approx 1.349$. In searching for such matchings in the phase diagram, there exist certain values of $x_*(2)$ starting from which numerical solutions $v(x)$ and $\alpha(x)$ cannot reach $x_F = 1$; the corresponding $v(x)$ will curve upward and quickly run into the sonic critical line again.

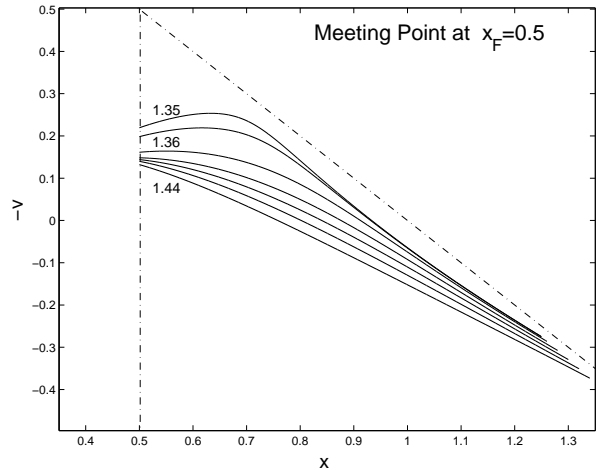


Figure 9. Backward integrations from a type 2 eigensolution at $x_*(2)$; those that can reach $x_F = 0.5$ are shown. The labelled numbers indicate the values of $x_*(2)$. The corresponding locus of α versus v are shown in Fig. 7 as solid circles.

(22). The corresponding $v - \alpha$ phase diagram is displayed in Fig. 8. It is clear that there exists a discrete solution match between $x_*(1) \approx 0.632$ and $x_*(2) \approx 1.349$. By selecting different meeting point x_F , one can search for other ranges of $x_*(1)$ and $x_*(2)$ for possible solution matches but none was found in our numerical exploration. The $v - \alpha$ phase locus of those numerical integrations that can reach $x_F = 0.5$ come very close to but do not intersect the $v - \alpha$ phase lo-

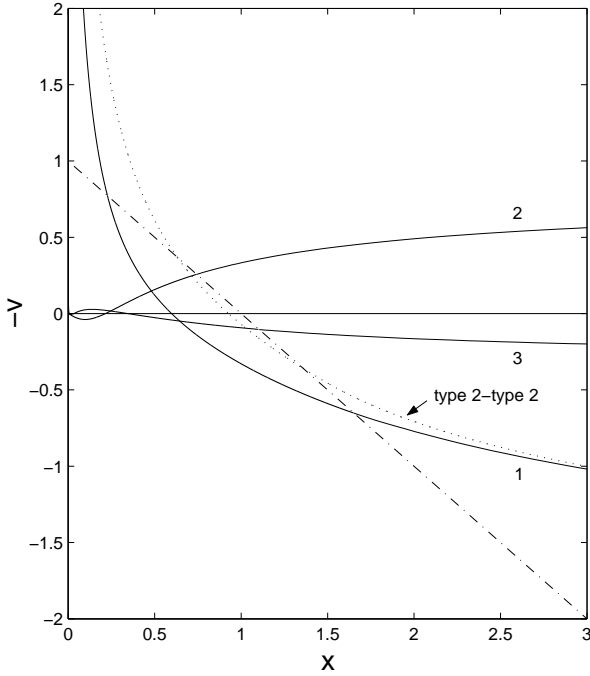


Figure 10. The first three discrete type 2-type 1 self-similar solutions [$v(x)$ versus x all denoted by light solid curves] crossing twice the sonic critical line, the dash-dotted line for $x - v = 1$, analytically and one type 2-type 2 similarity solution, denoted by the dotted curve, that also crosses twice the sonic critical line. Numerals 1, 2, 3 labelled along the three solid curves denote the number of stagnation points (i.e. $v = 0$) at the x -axis. All these similarity solutions diverge, approaching minus infinity as $x \rightarrow 0^+$ that are displayed more explicitly in Fig. 11 with the x -axis in a logarithmic scale.

cus determined from $x_*(1)$ (see Figs. 7 and 9). In short, the solution which passes consecutively the first sonic critical point at $x_*(1) \approx 0.632$ in the first quadrant and the second sonic critical point at $x_*(2) \approx 1.349$ in the fourth quadrant is a unique type 2-type 2 self-similar solution being analytic at both sonic critical points; and this solution has only one stagnation point across the x -axis. For completeness, we further integrate from the relevant $x_*(2)$ towards $x \rightarrow +\infty$ in terms of the type 2 solution (see dotted curve in Fig. 10).

By numerical exploration and analysis, we obtained discrete EECC self-similar solutions within the entire range of $0 < x < +\infty$, each crossing twice the sonic critical line analytically in the first and fourth quadrants. For all these self-similar solutions, the $x \rightarrow 0^+$ profiles have asymptotic diverging behaviours (17) and the $x \rightarrow +\infty$ profiles have asymptotic behaviours (16). The basic solution profile of the first (labelled by numeral 1 in Fig. 10) type 2-type 1 similarity solution with one stagnation point is qualitatively similar to its counterparts without crossing the sonic critical line as shown in Fig. 3 (i.e. curves with $V = 2, A = 6, 8, 10$, respectively). Furthermore, the family of type 2-type 1 solutions is very similar to Hunter’s solution family; two major differences are: (1) the condition at the origin $x = 0$ has been changed from $v \rightarrow 0$ to $v \rightarrow -\infty$; (2) the solutions are obtained in the ‘semi-complete’ space instead of ‘com-

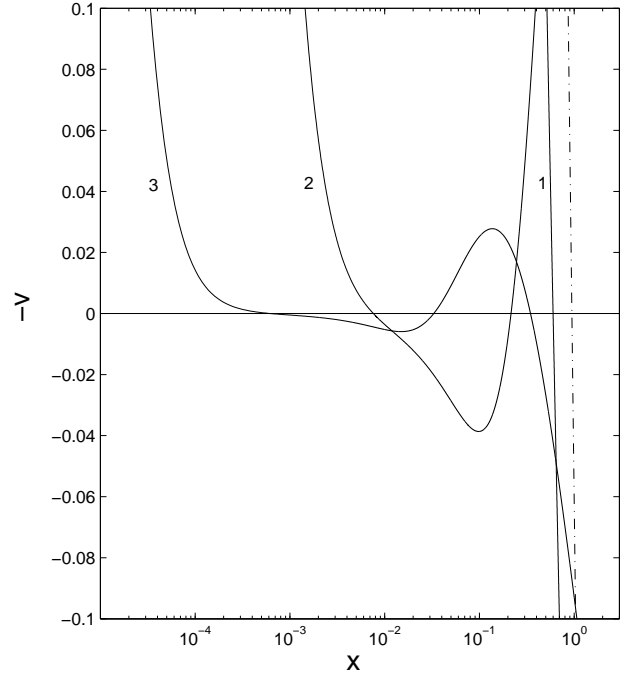


Figure 11. The enlarged portions of solution curves near the origin $x = 0$ of Fig. 10, showing the diverging behaviours and the number of stagnation points of discrete type 2-type 1 similarity solutions as $x \rightarrow 0^+$. The x -axis is shown in a logarithmic scale here. The dash-dotted line is the sonic critical line $x - v = 1$. Physically, these profiles represent subsonic radial oscillations in a self-similar manner.

plete’ space. In contrast to the ‘accretion solutions’ free of any sonic critical point described in subsection 8.2 of Boily & Lynden-Bell (1995), our novel EECC similarity solutions go across the sonic critical line twice and apparently have been missed by earlier investigations on isothermal collapses and flows with spherical symmetry.

We note again that a numerical integration backward from $x_*(2)$ along the primary direction is extremely sensitive to initial values. Thus, the accuracy of the type 2-type 2 similarity solution obtained may be improved, and there might still be matches at $x_F = 0.5$ if other initial steps away from $x_*(2)$ were chosen. For example, if one chooses a step of 0.001 away from $x_*(2)$ and integrates backward using a type 2 eigensolution to $x_F = 0.5$, it might be possible to find one or more intersections with those integrated from $x_*(1)$. Furthermore, solutions along the primary direction, with so many possible non-analytic ones tangential to the same direction, might be unstable (e.g. Ori & Piran 1988; Lai & Goldreich 2000) and might be physically irrelevant. In Section 4, we shall mainly focus on the type 2-type 1 self-similar solutions with eigensolutions along the secondary direction at $x_*(2)$.

4 ENVELOPE EXPANSION WITH CORE COLLAPSE (EECC) SOLUTIONS

We have examined the similarity solution structure in Section 3. We now divide all solutions extended through $0 < x < +\infty$ into two major classes. Among the two classes, each solution is continuous and smooth within the entire range of x . For x approaches infinity, a solution is determined by solution (16), that is, the reduced velocity $v(x)$ approaches a constant value V and the reduced mass density $\alpha(x)$ scales as A/x^2 asymptotically; when x approaches the origin, the solutions are determined either by solution (17) as a free-fall state with a reduced core mass m_0 or by condition (18) of vanishing velocity and finite α . The first group is referred to as Class I similarity solution and the second group is referred to as Class II similarity solution. For the structure of possible similarity solutions, we focus on Class I similarity solutions.

The Class I similarity solutions can be further divided into three subclasses based on the signs of the asymptotic radial speed parameter V . We denote by Class Ia similarity solutions for $V > 0$, by Class Ib similarity solutions for $V = 0$ and by Class Ic similarity solutions for $V < 0$, respectively. The Class Ib similarity solutions were studied previously by Shu (1977) as infall similarity solutions with an important limiting solution, the ‘expansion-wave collapse’ solution. Recently, these solutions (with $V = 0$ and $A < 2$) have been used to construct shocked LP-solutions to model ‘champagne flows’ in HII regions surrounding newborn stars (Shu et al. 2002). The Class Ic similarity solutions are core-collapse solutions with inflows at large radii. In contrast, the existence of Class Ia similarity solutions is a new revelation. Such similarity solutions describe situations that for a given r , the radial flow may be outward at a certain time, undergo one or more oscillations, and eventually collapse towards the central core in a nearly free-fall manner. It also describes a spherical fluid system under self-gravitation at a given instant t that its interior is core collapsing while its exterior envelope is expanding with or without subsonic radial oscillations in between. For this reason, we refer to the Class Ia solutions as ‘envelope expansion with core collapse’ (EECC) solutions.^{§§}

4.1 Physical Interpretations

We now focus on the physical meaning of the EECC self-similar solutions and examine specifically such EECC solutions with only one stagnation point along the x -axis. In the scenario of Shu (1977), the ‘expansion-wave collapse’ solution is constructed by joining two solutions at $x_* = 1$ with $\alpha(x)$ being continuous there. The $x < 1$ portion is the type 2 solution touching the sonic critical line at $x_* = 1$ and

^{§§} In describing early models of galactic winds, Holzer & Axford (1970) discussed steady-state solutions that may involve concurrent outflows and inflows given distributed sources of mass, momentum and energy (e.g. Burke 1968; Johnson & Axford 1971).

the $x \geq 1$ portion is simply the hydrostatic solution for a singular isothermal sphere (SIS). Such a solution physically describes a situation with a collapsing core approaching a free-fall state in the central region and with a hydrostatic exterior at rest for $x \geq 1$. The spherical surface separating the interior and exterior expands outward in a self-similar manner, at the speed of the isothermal sound a .

With this basic information in mind, the EECC self-similar solutions can be understood as follows. The interior portion ($x < \xi$, where ξ is the location of a surface of separation) is the infall/collapse region while the exterior portion ($x \geq \xi$) is the expansion region toward infinity. The outward movement of the exterior envelope leads to a wind with a constant speed at large radii. The spherical surface of separation $r_0 = \xi a t$ where the gas remains at rest travels outward as time goes on; this feature is similar to the ‘expansion-wave front’ of Shu (1977). The ‘expansion-wave collapse’ solution of Shu may also be regarded as a limiting case of our new EECC similarity solutions in the sense that the outer envelope is static at large x asymptotically rather than expanding or contracting at constant speeds. The travel speed of the expanding surface of separation is ξa , which is either subsonic for $\xi < 1$ [in cases of those EECC similarity solutions (e.g. Figs. 10 and 11) crossing the sonic critical line twice] or supersonic for $\xi > 1$ [in cases of those EECC similarity solutions (e.g. Fig. 3) that do not intersect the sonic critical line].

This explanation can be further extended to those EECC similarity solutions with more than one stagnation points, involving radial oscillations in the subsonic region. For such EECC similarity solutions, there exist more than one spherical surfaces of separation that expand outward with time. The distances between spherical surfaces of separation increase with time in a self-similar manner.

4.2 Astrophysical Applications

All similarity solutions in the range of $0^+ < x < +\infty$ are derived from nonlinear hydrodynamic equations and can be applied to various astrophysical systems with proper contexts. With necessary qualifications and adaptations, such EECC similarity solutions, which describe an outgoing envelope and a collapsing core may be applied to the late evolution stage of stars, for example, the asymptotic giant branch (AGB) phase or post-AGB phase before the appearance of a planetary nebula system. We have the following physical scenario in mind. A star (with a progenitor less than a few solar masses) swells enormously and sustains a massive wind with an asymptotic speed of $\sim 10 - 20 \text{ km s}^{-1}$. With an insufficient nuclear fuel supply from a certain epoch on, the central region starts to collapse while the outer envelope continues to expand. In a concurrent manner, the outer expansion removes stellar envelope mass, while the central infall and collapse produce a proto white dwarf at the center. Sufficiently away from initial and boundary conditions, the system may gradually evolve into a dynamic phase describable by an EECC similarity solution during a

timescale of a few hundred to several thousand years. Within this rough range of timescales, the accumulation of central core mass should not exceed the Chandrasekhar mass limit of $1.4M_{\odot}$ for a remnant white dwarf to survive; otherwise, a central explosion may occur within a planetary nebula. Meanwhile, the outer envelope expansion during the EECC phase can be faster than the pre-existing massive wind. This process will generally lead to formation of outward moving shock when a faster EECC outflow catches up a slower pre-existing wind. Theoretically, it is possible to construct shocked EECC similarity solutions to generalize the prior model results of Tsai & Hsu (1995) and Shu et al. (2002). We therefore suggest that the dynamical evolution of an EECC phase of around or less than a few thousand years may be the missing linkage between the AGB or post-AGB phase and the gradual appearance of a planetary nebula. Depending on physical parameters of the progenitor star, it might happen that the core collapse and subsequent central infalls during an EECC phase lead to a core mass exceeding the Chandrasekhar $1.4M_{\odot}$ and thus induce an explosion with an intensity determined by the actual rate of mass infall.

We now explore the utility of these EECC solutions obtained in this paper, including those that pass through the sonic critical line twice (Figs. 10 and 11) and those that do not involve critical points (Fig. 3). Relevant sets of parameters $\{A, V, m_0\}$ are summarized in Table 3 and the corresponding similarity solution curves of $\alpha(x)$, $v(x)$ and $m(x)$ versus x are presented in Figs. 12-15 (those curves for NoCP2, very close to the ones for NoCP3, were omitted to avoid cluttering). Those similarity solutions of ‘expansion wave’ type without involving critical points appear to give reduced core masses greater than 0.976 in general. In comparison, the type 2-type 1 EECC solutions can give rise to reduced core masses less than 0.976. For the type 2-type 1 EECC similarity solutions with more than one stagnation points (see Fig. 11), the reduced core mass parameter m_0 can be very small.

During the EECC similarity evolution, the core mass increases with time until the termination of the self-similar phase by other processes. To crudely estimate the final core mass near the end of the EECC phase, we have $G = 6.67 \times 10^{-8} \text{ cm}^3 \text{ g}^{-1} \text{ s}^{-2}$ and a typical timescale of $t = 3 \times 10^{10} \text{ s} \sim 10^3 \text{ yr}$ for the period between a late AGB phase and a beginning planetary nebula phase (e.g. Balick & Frank 2002). By transformation (5), the final core mass is given by $M(0, t) = a^3 m_0 / G$. For an isothermal sound speed $a = 20 \text{ km s}^{-1} = 2 \times 10^6 \text{ cm s}^{-1}$, the final core mass is $M(0, t) \sim 2 \times 10^3 m_0 M_{\odot}$. For a of the order of several km s^{-1} , the final core mass is approximately $\sim m_0 M_{\odot}$. Qualitatively, a smaller m_0 or a shorter period of the EECC phase would be necessary for a higher sound speed a without exceeding the Chandrasekhar mass limit of $1.4M_{\odot}$ for the central proto white dwarf. Within this scenario, it appears that type 2-type 1 EECC similarity solutions with more subsonic stagnation points are more likely of practical interest. For the CP2 EECC similarity solution (see Figs. 10, 11, 14 and Table 3), the outer envelope expands at large

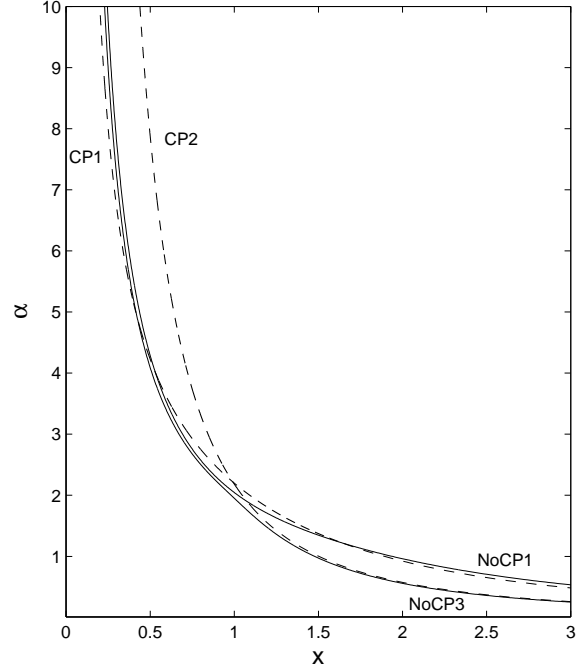


Figure 12. The curves of reduced density α versus x for several EECC similarity solutions in linear scales. The light solid curves NoCP1 and NoCP3 stand for those without crossing a sonic critical point, and the dashed curves CP1 and CP2 denote those crossing the sonic critical line twice, that is, the first and the third type 2-type 1 similarity solutions of Fig. 10. Note that the two light solid curves NoCP1 and NoCP3 are very close to each other for $x < 1$.

radii at a speed of ~ 0.3 times the sound speed (i.e. several km s^{-1}); the corresponding reduced core mass parameter m_0 is 1.2×10^{-5} .

For the problem at hand, the energy density \mathcal{E} and the energy flux density \mathcal{F} can be readily identified from the energy conservation equation (4)

$$\mathcal{E} = \frac{\rho u^2}{2} + a^2 \rho \left[\ln \left(\frac{\rho}{\rho_c} \right) - 1 \right] - \frac{1}{8\pi G} \left(\frac{\partial \Phi}{\partial r} \right)^2, \quad (23)$$

$$\mathcal{F} = u \rho \left[\frac{u^2}{2} + a^2 \ln \left(\frac{\rho}{\rho_c} \right) \right].$$

By using similarity transformation (5) for dependent variables and relations (7) and (12), we further obtain

$$\begin{aligned} \mathcal{E} &= \frac{a^2}{8\pi G t^2} \left[\alpha v^2 + 2\alpha \left(\ln \frac{\alpha}{4\pi G t^2 \rho_c} - 1 \right) - \alpha^2 (x - v)^2 \right], \\ \mathcal{F} &= \frac{a^3}{8\pi G t^2} \left(\alpha v^3 + 2\alpha v \ln \frac{\alpha}{4\pi G t^2 \rho_c} \right). \end{aligned} \quad (24)$$

For an actual astrophysical system, one may then use equations (23) and (24) to estimate relevant energy density and energy flux density, respectively.

5 DISCUSSION

In this paper, we investigated the spherical self-similar solutions for self-gravitating isothermal flows in the ‘semi-

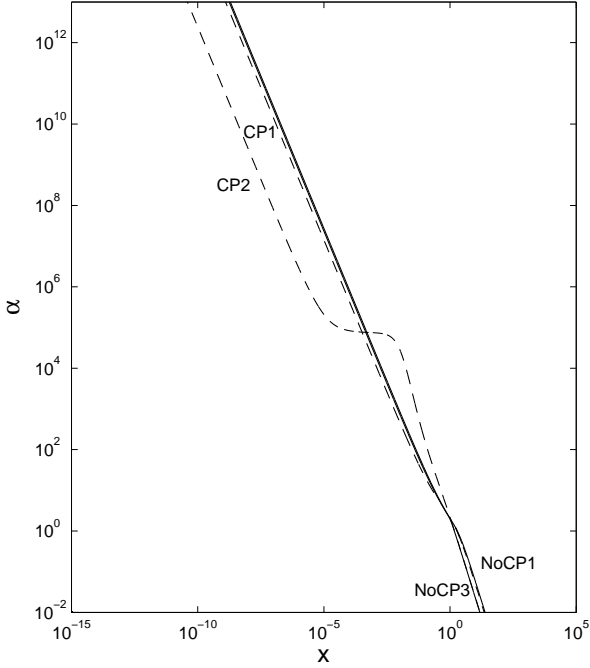


Figure 13. The curves of reduced density α versus x for the same EECC similarity solutions in Fig. 12 but in logarithmic scales. Note that $\alpha \rightarrow 0^+$ for $x \rightarrow +\infty$ and $\alpha \rightarrow +\infty$ for $x \rightarrow 0^+$. The rates of the asymptotic behaviours are different. The apparent wiggle in $\alpha(x)$ of CP2 dashed curve corresponds roughly to the range of the three stagnation points of type 2-type 1 solution labelled by numeral 3 in Figs. 10 and 11.

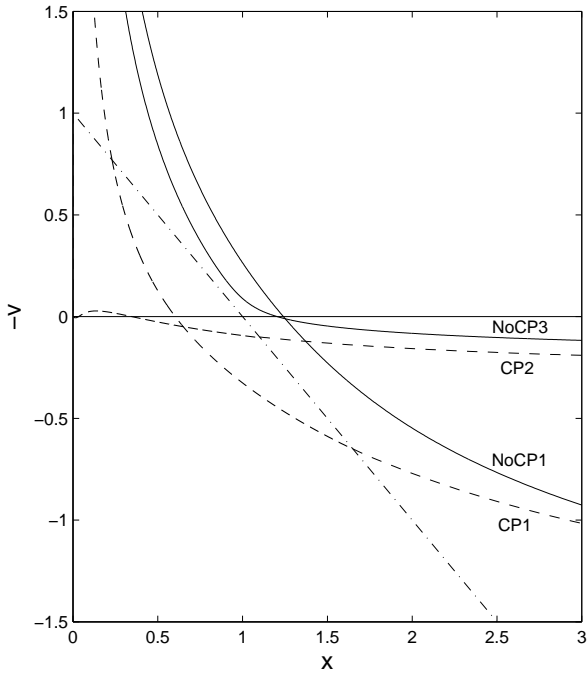


Figure 14. The curves of $-v$ versus x for the same EECC similarity solutions of Fig. 12 in linear scales. In addition to the two type 2-type 1 similarity solutions labelled by 1 and 3 of Fig. 10 displayed in dashed curves here, we also show two solutions without crossing the sonic critical point in light solid curves. The curve $v(x)$ for CP2 goes to $-\infty$ as $x \rightarrow 0^+$, as shown in Fig. 11.

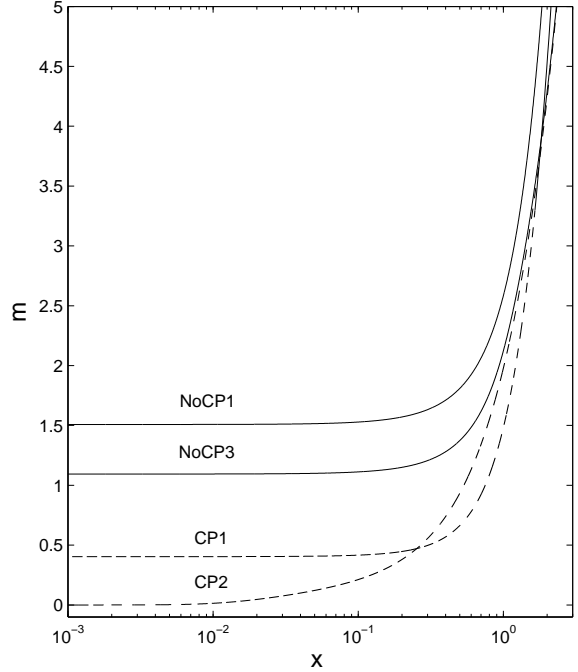


Figure 15. The curves of reduced enclosed mass m versus x for the same EECC similarity solutions of Fig. 12 in logarithmic scale for x axis. Each approaches a finite core mass parameter m_0 as $x \rightarrow 0^+$ (see Table 3 for relevant parameters).

Description	V	A	m_0
NoCP1	2.000	6.000	1.508
NoCP2	0.200	2.500	1.548
NoCP3	0.200	2.300	1.094
CP1	1.845	5.158	0.406
CP2	0.287	2.371	1.200×10^{-5}

Table 3. Parameters V , A and m_0 for the EECC similarity solutions; CP for solutions involving critical points and NoCP for solutions without critical points.

complete solution space' extending from the initial instant $x \rightarrow +\infty$ to the final instant $x \rightarrow 0^+$. The relevant similarity solutions are obtained and classified to compare with previous solutions and analyses [Larson 1969a; Penston 1969a; Shu 1977; Hunter 1977; Whitworth & Summers 1985 (WS)].

The novel class of infinitely many similarity solutions obtained in this paper, i.e., the EECC self-similar solutions and the envelope contraction with core collapse (EECC) self-similar solutions (e.g. solution labelled 2 in Figs. 10 and 11 that passes the sonic critical line twice with specific parameters $V = -0.766$, $A = 1.209$ and $m_0 = 5.171 \times 10^{-4}$), is constructed in the 'semi-complete solution space'. This is to be compared with the similarity solutions derived in the 'complete solution space' first introduced by Hunter (1977). By the invariance property under time reversal in this classical problem, these new self-similar solutions may be formally extended to the 'complete solution space' by properly joining two separate branches in the first and fourth quadrants of the 'semi-complete solution space' but with diverg-

ing asymptotic behaviours of $v(x)$ and $\alpha(x)$ at $t \rightarrow -\infty$. Similarity solutions without crossing the sonic critical line as shown in Figs. 2 and 3 also carry ECCC and EECC features, respectively, and are much easier to construct technically in the isothermal approximation; in a polytropic gas with various laws of radiative losses, some qualitatively similar features were mentioned in subsection 8.2 of Boily & Lynden-Bell (1995).

Regarding the isothermal approximation, the core collapsing (CC) portion may be justified qualitatively on the ground that the gas would heat up by adiabatic compressions. In the presence of a sufficient amount of radiative agents in a relatively high density region involving more frequent collisions, such radiative cooling processes may sustain an approximate condition of quasi-constant temperature. To sustain an isothermal condition for the envelope expansion (EE) portion, some heating mechanisms are necessary to compensate the inevitable cooling resulting from adiabatic expansions. Naturally, radiations from gas in the CC portion can be absorbed by gas in the EE portion to heat up the latter to some extent (depending on the escape efficiency of photons). In the astrophysical context of star formation, a gas cloud can be submerged in an intense electromagnetic radiation field when the nuclear reaction has been ignited in the central protostar. In such a situation, the large-scale gas cloud dynamics of contraction and expansion may be regarded as quasi-isothermal. Similar conditions may be applicable in the emergence of a planetary nebula system as well as in a certain evolution phase for hot gas in a galaxy cluster. Although not fully understood in details, there are other possible heating processes that may happen in the EE portion such as micro-turbulence, flow instabilities, shocks, wave dampings and magnetic fields etc.

With these considerations in mind, it is worthwhile to note that the isothermal assumption is a special case of the more general polytropic approximation (Cheng 1978; Goldreich & Weber 1980; Bouquet et al. 1985; Yahil 1983; Suto & Silk 1988; Maeda et al. 2002; Harada et al. 2003). Asymptotic solutions parallel to those of (16) – (18) as well as eigen-solutions across the sonic critical line can be readily derived. Therefore, EECC self-similar solutions in the polytropic approximation can be obtained with combined numerical and analytical analyses. One major difference is that, in the polytropic approximation, the asymptotic solution takes the form of

$$v \rightarrow Vx^{(1-\Gamma)/(2-\Gamma)}, \quad (25)$$

$$\alpha \rightarrow Ax^{-2/(2-\Gamma)}, \quad (26)$$

$$m \rightarrow Dx^{(4-3\Gamma)/(2-\Gamma)}, \quad (27)$$

where $x \propto rt^{(\Gamma-2)}$ is the independent similarity variable, Γ is the polytropic index, and V , A and D are three constant coefficients to the leading order. For $1 < \Gamma < 2$, the radial flow speed (either outflows or inflows) vanishes as $x \rightarrow +\infty$. For a finite radial range, the basic concept of

EECC similarity solutions advanced in this paper remains valid. Additional similarity solution features such as shocks, subsonic radial oscillations, central core collapse etc. are also expected. Polytropic EECC similarity solutions should have a wider range of astrophysical applications with, at least, one more degree of flexibility (i.e. Γ parameter).

Conceptually, the EECC similarity solutions provide a simple model scenario for the concurrence of inner infalls (including central core collapses) and outer envelope outflows (including asymptotic winds) with the separation surface (or stagnation point) travelling outward at a constant speed. In any self-gravitating spherical fluid system, the emergence of an EECC similarity phase depends upon allowed physical conditions that can be reached via a certain set of initial/boundary conditions of density and velocity at some time ago through other processes that were usually not self-similar.

For applications of the EECC similarity solutions, as well as other similarity solutions, we have noted several potential areas. The first one is the dynamical evolution phase connecting the AGB or post-AGB phase and the proto-planetary nebula (PN) phase, where the central core collapse to form a proto white dwarf and the envelope wind to create various PN morphologies are expected to happen simultaneously in a timescale of $\sim 10^3$ yrs (e.g. Balick & Frank 2002). By this process, a late-type star can continue to lose its envelope mass while forming a compact object at the collapsing core. After the self-similar phase, the system continues to evolve in a detached manner with the core and envelope separated. Shocks can be introduced either at the end of the AGB phase (Kwok 1982, 1993) when the faster envelope expansion during the EECC phase catches up with the slower pre-existing wind or when infalling materials bounced back from the central compact object. Much as Tsai & Hsu (1995) and Shu et al. (2002) introduced shocks to the similarity solutions in star formation and ‘champagne flows’ of HII regions, one can construct EECC similarity solutions with shocks in the context of planetary nebulae. The solutions other than the EECC ones (including their time-reversal counterparts) have been used in star-formation as well as other gravitational collapse and flow problems.

For astrophysical systems of even larger scales such as clusters of galaxies (e.g. Sarazin 1988; Fabian 1994), the similarity solutions can be valuable for understanding a certain phase of their evolution. Specifically, if their evolution involves a self-similar phase of central collapse (e.g. Gunn & Gott 1972; Fillmore & Goldreich 1984; Bertschinger 1985; Navarro et al. 1997), then isothermal similarity solutions (17) and (18) seem to suggest two possible classes of galaxy clusters that emit X-rays through hot gases virialized in gravitational potential wells, namely, those with steep gravitational potential wells and thus extremely high X-ray core luminosities, and those with relatively smooth and shallow gravitational potential wells and thus normal X-ray core luminosities.

Finally, we note that the stability of similarity solutions is of interest in various contexts. As several authors have de-

clared (Ori & Piran 1988; Hanawa & Nakayama 1997), some self-similar solutions may not be stable when one performs a normal mode analysis. The instability growth rates are different for various types of similarity solutions in general. At this moment, the stability problem for the EECC similarity solution remains open for future research. In some cases, depending on the growth rates, an unstable EECC similarity solution might be of interest to disrupt a self-similar phase within proper timescales. For example, we do not expect a self-similar phase to last forever, especially for the ephemeral phase of $\sim 10^3$ yrs between the end of AGB phase and the PN phase (Kwok 1982, 1993; Balick & Frank 2002).

ACKNOWLEDGMENTS

This research has been supported in part by the ASCI Center for Astrophysical Thermonuclear Flashes at the University of Chicago under Department of Energy contract B341495, by the Special Funds for Major State Basic Science Research Projects of China, by the Tsinghua Center for Astrophysics, by the Collaborative Research Fund from the National Natural Science Foundation of China (NSFC) for Young Outstanding Overseas Chinese Scholars (NSFC 10028306) at the National Astronomical Observatory, Chinese Academy of Sciences, and by the Yangtze Endowment from the Ministry of Education through the Tsinghua University. Affiliated institutions of Y.Q.L. share the contribution.

APPENDIX A: ASYMPTOTIC SOLUTIONS

In this Appendix, we describe and summarize asymptotic behaviours of similarity solutions for $x \rightarrow +\infty$ and $x \rightarrow 0^+$, and for Taylor expansions across the sonic critical line.

A1 Asymptotic solutions for $x \rightarrow +\infty$

As $x \rightarrow +\infty$ (i.e. at an initial instant $t \rightarrow 0^+$), a sensible physical requirement is that the radial flow speed and fluid density should remain finite. It turns out that for a finite $v(x)$, the reduced density $\alpha(x)$ scales as $\propto x^{-2}$. The Taylor series of $v(x)$ and $\alpha(x)$ for $x \rightarrow +\infty$ can be written as

$$v = v_0 + v_1 x^{-1} + v_2 x^{-2} + v_3 x^{-3} + \dots, \quad (\text{A1})$$

$$\alpha = a_2 x^{-2} + a_3 x^{-3} + a_4 x^{-4} + \dots,$$

where v_i ($i = 0, 1, 2, \dots$) and a_j ($j = 2, 3, \dots$) are series expansion coefficients. By substituting these expressions into nonlinear ODEs (9) and (10), one can determine expansion coefficients v_i and a_j by comparing powers of x in order. The first several terms are given explicitly in equation (16). As expected, the series expansion involves two independent parameters V and A as initial conditions. The parameter V describes the asymptotic radial flow speed and can take either positive or negative values. The parameter A describes the asymptotic density distribution $\rho_0 = Aa^2/(4\pi Gr^2)$, corresponding to a singular isothermal sphere (SIS) if applied

to the entire radial range. For different values of V and A , one can introduce various conditions to initiate self-similar processes.

A2 Asymptotic solutions for $x \rightarrow 0^+$

The asymptotic solution behaviours for $x \rightarrow 0^+$ (i.e. the final moment of $t \rightarrow +\infty$ at a given r) can be derived in the same manner as $x \rightarrow +\infty$. For the reduced velocity $v(x)$, it may either diverge (in an almost free-fall state) or vanish for $x \rightarrow 0^+$. We therefore obtain two sets of asymptotic solutions (17) and (18), keeping only the leading-order terms. In particular, solution (17) describes a free-fall state with a reduced core mass parameter m_0 .

A3 Taylor expansions across the sonic critical line

As the techniques of obtaining eigensolutions across the sonic critical line have been discussed in WS and Hunter (1986), we state the basic results below.

A3.1 Eigensolutions across the sonic critical line

When the coefficients of $dv(x)/dx$ and $d\alpha(x)/dx$ vanish on the left-hand sides of nonlinear ODEs (9) and (10), it is necessary to impose condition (15) in order to derive finite $dv(x)/dx$ and $d\alpha(x)/dx$. Specifically, derivatives of $v(x)$ and $\alpha(x)$ can be computed through the L'Hôpital's rule, and two types of eigensolutions analytic across the sonic critical line can be derived. In addition to expressions (19) and (20), we summarize higher-order derivatives below. For type 1 solutions, we have at the sonic critical point $x = x_*$

$$\begin{aligned} \left. \frac{d^2 v}{dx^2} \right|_{x=x_*} &= -\frac{(x_* - 1)(x_* - 3)}{x_*^2(x_* - 3)}, \\ \left. \frac{d^2 \alpha}{dx^2} \right|_{x=x_*} &= \frac{2(x_*^2 - 8x_* + 13)(x_* - 3)}{x_*^3(x_* - 3)}, \\ \left. \frac{d^3 v}{dx^3} \right|_{x=x_*} &= \frac{(x_* - 1)(x_*^2 - 3x_* + 6)(x_* - 3)^2}{x_*^3(x_* - 3)^2(x_* - 4)}, \\ \left. \frac{d^3 \alpha}{dx^3} \right|_{x=x_*} &= \frac{2(x_* - 2)(x_*^3 - 19x_*^2 + 93x_* - 147)(x_* - 3)^2}{x_*^4(x_* - 3)^2(x_* - 4)}, \end{aligned} \quad (\text{A2})$$

and for type 2 solutions, we have

$$\begin{aligned} \left. \frac{d^2 v}{dx^2} \right|_{x=x_*} &= \frac{x_*^2 - 5x_* + 5}{x_*^2(2x_* - 3)}, \\ \left. \frac{d^2 \alpha}{dx^2} \right|_{x=x_*} &= -\frac{2(x_*^2 - 6x_* + 7)}{x_*^3(2x_* - 3)}, \\ \left. \frac{d^3 v}{dx^3} \right|_{x=x_*} &= -\frac{6x_*^5 - 16x_*^4 - 58x_*^3 + 266x_*^2 - 345x_* + 150}{x_*^3(2x_* - 3)^2(3x_* - 4)}, \\ \left. \frac{d^3 \alpha}{dx^3} \right|_{x=x_*} &= \frac{6(x_* - 2)(2x_*^4 + 2x_*^3 - 42x_*^2 + 83x_* - 47)}{x_*^4(2x_* - 3)^2(3x_* - 4)}. \end{aligned} \quad (\text{A3})$$

The corresponding Taylor expansions can then be constructed for the two types of eigensolutions across the sonic

critical line. We immediately note that there are critical points where higher-order derivatives diverge, e.g. $x_* = 4$ for denominators of the third-order derivatives of type 1 solutions in equation (A2); $x_* = 3/2$ in the denominator of the second-order derivatives of type 2 solutions in equation (A3); and $x_* = 3/2$ and $4/3$ in the denominator of the third-order derivative of type 2 solution and so forth. In general, for $x_* = 1 + N$ with integer $N \geq 2$, the L'Hôpital's rule fails for type 1 eigensolutions (e.g. $x_* = 3$ in equation A2); while for $x_* = 1 + 1/N$ with integer $N \geq 2$, the L'Hôpital's rule fails for type 2 eigensolutions (see section 3 of Hunter 1986). To avoid such densely distributed divergent points as $x \rightarrow 1^+$ for type 2 eigensolutions, it would be wise to use up to second-order derivatives with a properly chosen step away from x_* .

A3.2 Classification of saddle and nodal critical points

There exist two types of sonic critical points (Jordan & Smith 1977), the saddle and nodal points. The classification of these two types is based on the topological structure of solution paths around the sonic critical point (WS). In short, the critical point is a saddle point when the two gradients of eigensolutions $v(x)$ are of the opposite signs; while the critical point is a nodal point when the two gradients carry the same sign (Jordan & Smith 1977). In our problem, the critical points with $0 < x_* < 1$ are saddle points, while those with $x_* > 1$ are nodal points; the special case of $x_* = 1$ is degenerate.

Mathematically allowed solutions across a sonic critical point are different for saddle and nodal points. Across a saddle critical point, similarity solutions can pass through via the two eigensolutions. For a node, besides the two eigensolutions, infinitely many solutions can go cross the node along the primary direction, that is, they all cross the node tangentially to the eigensolution with a larger absolute value of gradient for $v(x)$. Hunter (1986) noted that the two eigensolutions are analytic while others are not.

Numerical integrations away from a saddle or a node along the secondary direction [i.e. in terms of the eigensolution with smaller absolute value of gradient for $v(x)$] are stable or neutrally stable, respectively; while numerical integrations away from a node along the primary direction are unstable due to numerous path branches at the node in that direction. The key is to choose a proper integration step away from the node and pertinent initial values for numerical integrations along the primary direction.

A3.3 Weak discontinuities

There are two important aspects to allow weak discontinuities in similarity solutions across a nodal critical point (Lazarus 1981; Whitworth & Summers 1985). The first one is to allow for those non-analytic similarity solutions along the primary direction across a node. The second one is to allow linear combinations (in the local sense) of the two eigensolutions at a node, i.e. the combined gradient is between

those of the two eigensolutions (WS). In this manner, WS have obtained their continuous bands of similarity solutions. Weak discontinuities in similarity solutions, as claimed by Hunter (1986), may bear little physical significance. Mathematically, we simply point out here the possibility of constructing WS types of band solutions from discrete EEC as well as ECCC self-similar solutions.

REFERENCES

- Balick B., Frank A., 2002, *ARA&A*, 40, 439
 Bertschinger E., 1985, *ApJS*, 58, 39
 Boily C. M., Lynden-Bell D., 1995, *MNRAS*, 276, 133
 Bonner W. B., 1956, *MNRAS*, 116, 351
 Bouquet S., Feix M. R., Fijakow E., Munier A., 1985, *ApJ*, 293, 494
 Burke J. A., 1968, *MNRAS*, 140, 241
 Chandrasekhar S., 1957, *Stellar Structure*. Dover Publications, New York
 Cheng A. F., 1978, *ApJ*, 221, 320
 Courant R., Friedrichs K. O., 1948, *Supersonic Flow and Shock Waves*. Springer-Verlag, New York
 Ebert R., 1955, *Zs. Ap.*, 37, 217
 Fan Z. H., Lou Y. Q., 1999, *MNRAS*, 307, 645
 Fabian A. C., 1994, *ARA&A*, 32, 277
 Fillmore J. M., Goldreich P., 1984, *ApJ*, 281, 1
 Foster P. N., Chevalier R. A., 1993, *ApJ*, 416, 303
 Goldreich P., Weber S. V., 1980, *ApJ*, 238, 991
 Gunn J. E., Gott III J. R., 1972, *ApJ*, 176, 1
 Hanawa T., Nakayama K., 1997, *ApJ*, 484, 238
 Harada T., Maeda H., Semelin B., 2003, *Phys. Rev. D*, 67, 084003
 Hayashi C., 1966, *ARA&A*, 4, 171
 Holzer T. E., Axford W. I., 1970, *ARA&A*, 8, 31
 Hunter C., 1967, in *Relativity Theory and Astrophysics 2. Galactic Structure*, ed. J. Ehlers (Providence: American Mathematical Society), p. 169
 Hunter C., 1977, *ApJ*, 218, 834
 Hunter C., 1986, *MNRAS*, 223, 391
 Johnson H. E., Axford W. I. 1971, *ApJ*, 165, 381
 Jordan D. W., Smith P., 1977, *Nonlinear Ordinary Differential Equations*. Oxford Univ. Press, Oxford
 Kwok S., 1982, *ApJ*, 258, 280
 Kwok S., 1993, *ARA&A*, 31, 63
 Lai D., 2000, *ApJ*, 540, 946
 Lai D., Goldreich P., 2000, *ApJ*, 535, 402
 Landau L. D., Lifshitz E. M., 1959, *Fluid Mechanics*. Pergamon Press, New York
 Larson R. B., 1969a, *MNRAS*, 145, 271
 Larson R. B., 1969b, *MNRAS*, 145, 405
 Larson R. B., 1973, *ARA&A*, 11, 219
 Lazarus R. B., 1981, *SIAM Journal on Numerical Analysis*, 18, 316
 Lynden-Bell D., Lemos J. P. S., 1988, *MNRAS*, 233, 197
 Lemos J. P. S., Lynden-Bell D., 1989a, *MNRAS*, 240, 303
 Lemos J. P. S., Lynden-Bell D., 1989b, *MNRAS*, 240, 317
 Maeda H., Harada T., Iguchi H., Okuyama N., 2002, *Progress of Theoretical Physics*, 108, 819
 Mestel L., 1974, in *Magnetohydrodynamics (Geneva Observatory)*, pp. 116-150
 Navarro J. F., Frenk C. S., White S. D. M., 1997, *ApJ*, 490, 493
 Ori A., Piran T., 1988, *MNRAS*, 234, 821
 Penston M. V., 1969a, *MNRAS*, 144, 425
 Penston M. V., 1969b, *MNRAS*, 145, 457
 Sarazin C. L., 1988, *X-Ray Emissions from Clusters of Galaxies*. Cambridge University Press, Cambridge

- Sedov L. I., 1959, *Similarity and Dimensional Methods in Mechanics*. Academic, New York
- Shu F. H., 1977, *ApJ*, 214, 488
- Shu F. H., Adams F. C., Lizano S., 1987, *ARA&A*, 25, 23
- Shu F. H., Lizano S., Galli D., Cantó J., & Laughlin G., 2002, *ApJ*, 580, 969
- Spitzer L., 1968, in *Nebulae and Interstellar Matter*, ed. B. M. Middlehurst and L. H. Aller (Chicago: University of Chicago Press), p.1
- Spitzer L., 1978, *Physical Processes in the Interstellar Medium*. Wiley, New York
- Suto Y., Silk J., 1988, *ApJ*, 326, 527
- Tsai J. C., Hsu J. J. L., 1995, *ApJ*, 448, 774
- Whitworth A., Summers D., 1985, *MNRAS*, 214, 1
- Yahil A., 1983, *ApJ*, 265, 1047